Bacterial surface lipoproteins mediate epithelial microinvasion by *Streptococcus pneumoniae*

Jia Mun Chan[a#], Elisa Ramos-Sevillano[b], Modupeh Betts[a]*, Holly U. Wilson[a], Caroline M. Weight[a]**, Ambrine Houhou-Ousalah[a], Gabriele Pollara[a], Jeremy S. Brown[b], Robert S. Heyderman[a#]

[a] Research Department of Infection, Division of Infection and Immunity, University College London, London, UK.
[b] Department of Respiratory Medicine, Centre for Inflammation and Tissue Repair, University College London, London, United Kingdom

Running title: Pneumococcal lipoproteins in epithelial microinvasion

Address correspondence to Robert S. Heyderman, r.heyderman@ucl.ac.uk or Jia Mun (Elizabeth) Chan, elizabeth.jm.chan@ucl.ac.uk.

* Present address: Institute of Infection, Veterinary and Ecological Sciences, University of Liverpool, Liverpool, UK.
** Present address: Department of Biomedical and Life Sciences, Lancaster University, Lancaster, UK.

Keywords: *Streptococcus pneumoniae*, host-microbe interactions, microinvasion, bacterial lipoproteins, epithelium

Abstract word count: 241 words.
Importance word count: 129 words.
Manuscript word count: 5699 words.

ABSTRACT

Streptococcus pneumoniae, a common coloniser of the upper respiratory tract, invades nasopharyngeal epithelial cells without causing disease in healthy participants of controlled human infection studies. We hypothesised that surface expression of pneumococcal lipoproteins, recognised by the innate immune receptor TLR2, mediate epithelial microinvasion. Mutation of *lgt* in serotype 4 (TIGR4) and serotype 6B (BHN418) pneumococcal strains abolishes the ability of the mutants to activate TLR2 signalling. Loss of *lgt* also led to concomitant decrease in interferon signalling triggered by the bacterium. However, only BHN418 *lgt::cm* but not TIGR4 *lgt::cm* was significantly attenuated in epithelial adherence and microinvasion compared to their respective wild-type strains. To test the hypothesis that differential lipoprotein repertoires in TIGR4 and BHN418 lead to the intraspecies variation in epithelial microinvasion, we employed a motif-based genome analysis and identified an additional 525 a.a. lipoprotein (pneumococcal accessory lipoprotein A; *palA*) encoded by BHN418 that is absent in TIGR4. The gene encoding *palA* sits within a putative genetic island present in ~10% of global pneumococcal isolates. While *palA* was enriched in carriage and otitis media pneumococcal strains, neither mutation nor overexpression of the gene encoding this lipoprotein significantly changed microinvasion patterns. In conclusion, mutation of *lgt* attenuates epithelial inflammatory responses during pneumococcal-epithelial interactions, with intraspecies variation in the effect on microinvasion. Differential lipoprotein repertoires encoded by the different strains do not explain these differences in microinvasion. Rather, we postulate that post-translational modifications of lipoproteins may account for the differences in microinvasion.

IMPORTANCE

Streptococcus pneumoniae (pneumococcus) is an important mucosal pathogen, estimated to cause over 500,000 deaths annually. Nasopharyngeal colonisation is considered a necessary prerequisite for disease, yet many people are transiently and asymptomatically colonised by pneumococci without becoming unwell. It is therefore important to better understand how the colonisation process is controlled at the epithelial surface.

Controlled human infection studies revealed the presence of pneumococci within the epithelium of healthy volunteers (microinvasion). In this study, we focused on the regulation of epithelial microinvasion by pneumococcal lipoproteins. We found that pneumococcal lipoproteins induce epithelial inflammation but that differing lipoprotein repertoires do not significantly impact the magnitude of microinvasion. Targeting mucosal innate immunity and epithelial microinvasion alongside the induction of an adaptive immune response may be effective in preventing pneumococcal colonisation and disease.

INTRODUCTION

Streptococcus pneumoniae (pneumococcus) is a versatile pathobiont capable of asymptomatically colonising the nasopharynx, causing localised infections of the middle ear, respiratory tract and lungs, and causing disseminated invasive disease (e.g. bacteraemic pneumonia and meningitis) with high mortality rates (1). *S. pneumoniae* has long been considered an extracellular pathogen despite demonstration of bacterial invasion *in vitro* using epithelial and endothelial cell lines (1). However, controlled human infection with a serotype 6B strain revealed that the pneumococcus invades the nasopharyngeal epithelium of healthy carriers, stimulating epithelial inflammation without causing overt symptoms or disease (2–4). We have termed this phenomenon microinvasion, which is distinct from the invasion of deeper tissues or dissemination systemically which characterise disease (2). Inflammation triggered by the epithelium-associated and intracellular bacteria, which peaks 9 days post inoculation, may be important for clearance and onward transmission (2).

In this study, we explored the hypothesis that surface expression of pneumococcal lipoproteins mediate epithelial microinvasion. Pneumococcal lipoproteins are post-translationally lipidated surface proteins, many of which function as metabolite transporters (5, 6). *S. pneumoniae* lipoproteins have also been shown to be major TLR2 ligands in macrophages, are required for a Th17 response and for many of the dominant macrophage gene transcriptional responses, such as induction of IRAK-4–dependent protective cytokines (7–9). *S. pneumoniae* encodes over 30 lipoproteins, including the bifunctional adhesin/manganese transporter PsaA and the peptidoglycan hydrolase DacB (5, 10–12). Blocking lipidation by mutating

the prolipoprotein diacylglyceryl transferase encoding gene *lgt* de-anchors lipoproteins from the cell surface, resulting in the release of immature preprolipoproteins into the extracellular milieu and abolishing the ability of the bacteria to activate TLR2 signalling (8, 9, 13). Mutating *lgt* also attenuates pneumococcal virulence and shortens colonisation duration in murine models (8, 14).

To explore whether heterogeneity in surface-expression of pneumococcal lipoproteins also explains the differences in microinvasion seen between strains, we blocked lipoprotein lipidation by inactivation of *lgt* in two well-characterized strains: a highly invasive strain (TIGR4, serotype 4) and a less invasive strain (BHN418, serotype 6B) which was used in the controlled human challenge experiments (15, 16). It is important to note that pneumococcal strains from both serotypes can asymptomatically colonise as well as cause invasive disease in susceptible hosts, albeit to different extents (17). While attenuation of inflammatory responses were seen with both serotype 6B and serotype 4 *lgt* mutants, we observed intraspecies differences in the contribution of lipoproteins to microinvasion, with greater effects of lipoproteins with the less invasive 6B strain. Genomic analysis revealed the presence of a previously uncharacterised lipoprotein encoded within a genetic island found in BHN418 and approximately 10% of pneumococcal strains, but not in TIGR4. We designate this protein pneumocccal accessory lipoprotein A, or PalA, and investigated its role in mediating intraspecies differences in microinvasion.

RESULTS

Pneumococcal *lgt* mutants induce lower levels of TLR2 and interferon signalling compared to than wild type strains. In line with previous reports, mutation of *lgt* in both TIGR4 and BHN418 completely abolished the ability of these strains to trigger TLR2 signalling in HEK-Blue^{TM} hTLR2 reporter cells, while genetic complementation of *lgt* at a chromosomal ectopic site restored WT-like ability to stimulate the TLR2 pathway (Figure 1A) (9). Although macrophages respond to pneumococcal infections by activating TLR2 signalling pathways, it is unknown if nasopharyngeal epithelial cells respond in the same way (8, 9, 18). Using a transcriptional module reflective of TLR2 signalling and previously published transcriptomic datasets (2, 19), we found evidence of elevated TLR2-mediated transcriptional activity in Detroit 562 nasopharyngeal epithelial cells infected with TIGR4 and BHN418 (Figure 1B; Supplementary Figure 1).

TLR2 activation is necessary for full induction of TLR4 by the *S. pneumoniae* virulence factor pneumolysin (20, 21). Transcriptomic analyses of human nasal biopsy samples from controlled pneumococcal challenge experiments and nasopharyngeal cell lines infected with *S. pneumoniae* also showed upregulation of interferon signalling (6, 7). We therefore hypothesize that TLR2 activation potentiates interferon signalling in epithelial cells triggered by *S. pneumoniae* infection. Using qPCR, we observed that Detroit 562 cells infected with TIGR4 *lgt::cm* have reduced expression of *CXCL10*, *IFNB1* and *IFNL1* compared to cells infected with WT TIGR4 (Figure 1C-E), while cells infected with BHN418 *lgt::cm* have reduced expression of *CXCL10* and *IFNL3* compared to those infected with WT BHN418 (Figure 1C,1F).

Our results suggest that lipoprotein-mediated TLR2 activation augments the epithelial interferon response during pneumococcal microinvasion.

Mutation of *lgt* attenuates epithelial microinvasion by *S. pneumoniae* serotype 6B but not by serotype 4. To determine if mutation of *lgt* and loss of TLR2 signalling impact on pneumococcal microinvasion, we infected confluent Detroit 562 nasopharyngeal cells (NPE) with serotype 6B (BHN418) and serotype 4 strains (TIGR4) for 3 hours (3 hpi), measuring the number of cell associated, intracellular and planktonic bacteria in the cell culture supernatant. Mutation of *lgt* significantly attenuated the ability of BHN418 but not TIGR4 to associate with and be internalised into Detroit 562 cells (Figure 2A-B, 2D-2E). In concordance with prior reports, serotype 4 strains were more invasive compared to serotype 6B strains, with ~5 times more intracellular WT TIGR4 recovered compared to WT BHN418 (Figure 2B, 2D) (15, 17). The *lgt* mutation also significantly reduced the number of planktonic BHN418 but not TIGR4 (Figure 2F).

Genetic complementation of *lgt* in the BHN418 *lgt::cm* mutant did not fully restore microinvasion of NPE cells to WT-like levels, despite complementation in the HEK-Blue^{TM} hTLR2 reporter assay (Figure 1A, Figure 2A-F). We double-checked the strain genotype using Illumina sequencing and confirmed *lgt* transcription (or lack thereof) in the TIGR4 and BHN418 strains using semi-quantitative PCR (Supplementary Table 1, Supplementary Figures 2A-B). Leaky expression of the P_{IPTG} promoter in the absence of inducer is sufficient to result in *lgt* expression (Supplementary Figures 2A-B). In agreement with prior studies, immunoblotting revealed substantially reduced retention but not complete loss of lipoproteins such as PiuA in whole cell lysates in the *lgt::cm* mutant compared to wild-type and

complementation strains (Supplementary Figures 3A-B) (13, 14). We conclude that the lack of complementation for the microinvasion phenotype is not due to failure in genetic complementation.

Mutation of *lgt* has been associated with growth defects in cation-limiting conditions, human blood and mouse bronchoalveolar lavage fluid (14). Fewer planktonic BHN418 *lgt* mutant bacteria were also recovered from our NPE infection experiments (Figure 2C). Time course sampling of planktonic pneumococci grown with Detroit 562 cells revealed a minor growth defect for the BHN418 *lgt* mutant starting at 3 hpi but not for the TIGR4 *lgt* mutant (Figure 3A-B). To determine if the growth defect was dependent on the presence of NPE cells, time course sampling of planktonic BHN418 and its *lgt* mutant grown in infection medium and rich THY medium were performed. The growth defect was replicated in cell-free medium and is therefore not dependent on the presence of NPE cells (Figure 3C-D).

Our results indicate that inactivation of Lgt and therefore the lipoprotein processing pathway had greater consequences for BHN418 compared to TIGR4, except in their ability to trigger epithelial inflammation. These observations suggest that activation of the TLR2 pathway during pneumococcal-epithelial interactions is not dependent on the number of cell-associated or intracellular pneumococci. Additionally, within the timeframe of our assays, TLR2 signalling neither promotes nor inhibits epithelial microinvasion by *S. pneumoniae*.

BHN418 encodes a novel lipoprotein absent in TIGR4. One potential explanation for the intraspecies differences in microinvasion upon *lgt* mutation is the presence of one or more lipoproteins in BHN418 which are absent in TIGR4. This lipoprotein may play a role as an adhesin and/or be important for nutrient transport and growth

during infections. To address this hypothesis, we used a motif-based sequence toolkit, the MEME Suite, to compare the lipoprotein repertoires of BHN418 and TIGR4 (22). We identified 43 open reading frames (ORFs) in TIGR4 and 44 ORFs in BHN418 with gene products that fit the criteria for a lipoprotein (detailed in Materials and Methods) (Table 1). Of these putative lipoprotein ORFs, only one is present in BHN418 but not in TIGR4. There are no lipoprotein ORFs present in TIGR4 that are not also present in BHN418.

The lipoprotein encoded by BHN418 but not TIGR4, encoded by the gene with the locus tag RSS80_03595 and which we named pneumococcal accesssory lipoprotein A (PalA), comprises of 525 amino acids with sequence and structural homology to extracellular solute binding domain proteins that deliver substrates to ABC family transporters (Figure 4A-B). We modeled PalA's tertiary structure using AlphaFold2 and PHYRE, revealing a Type II periplasmic binding protein-fold characterized by two subdomains connected with a hinge region (Figure 4B, Supplementary Figure 4A) (23–25). The two predicted structures aligned well with each other, barring small conformational differences in the accessibility of the potential substrate binding pocket (Supplementary Figure 4B-4C). The N-terminal extension (stalk like structure) seen in Figure 4B is likely cleaved post-lipidation (5).

Periplasmic (extracellular) binding proteins deliver substrates to ABC transporters, which are multi subunit proteins comprising of two transmembrane permease domains and two cytoplasmic ATPase domains (26). Two genes encoding ABC transporter permease domain proteins, annotated as *yteP* and *araQ*, were found ~3.3kb and ~2.4kb upstream of *palA.* We were unable to locate ORF(s) encoding for the ATPase domain proteins in the 10kb region upstream or downstream of *palA*. Taken together, PalA likely binds to and delivers substrate(s) to

YteP and/or AraQ. It is uncertain if YteP and/or AraQ co-opt the ATPase domains of ABC family transporters encoded elsewhere on the genome, in a similar strategy as the raffinose utilisation system, or no longer function as transporters (27, 28).

This genetic context suggests that *palA* is the fifth gene in an operon encoding for carbohydrate import and utilisation genes, which includes *yteP* and *araQ* (Figure 4A). Upstream of the operon is a gene encoding a putative transcriptional regulator, *ybbH,* which may play a role in regulating expression of the operon. The operon and *ybbH* sit within an 11.5 kb region with ~30% GC content, flanked by repetitive insertion sequences with homology to *IS630* elements. This region was likely acquired via horizontal gene transfer as the overall mean GC content of pneumococcal strains is around 40% (29). This putative genetic island is directly downstream of *spxB*, which encodes an important pneumococcal virulence factor involved in the production of H_2O_2 (30). Alignment of TIGR4 whole genome sequencing reads to the BHN418 genome revealed the absence of the entire putative island in the TIGR4 genome (Supplementary Figure 5 (29).

To determine if *palA* is predominantly present in more carriage-type serotypes, such as serotype 6B, we examined the presence of *palA* in a well-curated dataset of 2806 carriage isolates from Malawi (31). 567 of these carriage isolates (20.5%) carry *palA* in their chromosome. Mapping the analysis results onto a hierarchal clustering (Newick) tree showed that *palA* is present in specific lineages, with no clear association to capsular serotypes or sequence types (genetic relatedness, visualised as neighbouring branches on a Newick tree) (Supplementary Figure 6) (31). However, presence of *palA* is enriched in certain serotypes, particularly serotype 6A (39/93, 41.9%), 6B (12/31, 38.7%), 10A (29/34, 85%), 15B (52.76, 68.4%), 16F (60/94, 63.8%), 23B (45/103, 43.7%), 35A (28/28, 100%) and

35B (60/114, 52.6%) (Supplementary Table 2). Additionally, the branching patterns of the phylogenetic tree for the Malawi carriage isolates supports the inference that *palA* and its associated genetic island were acquired via horizontal gene transfer and expanded in specific lineages (Supplementary Figure 6).

PalA presence is enriched in carriage and ear isolates. Maintenance of this 11.5kb genetic island is potentially costly and suggests that the island confers some form of advantage to isolates that carry it. *S. pneumoniae* is capable of colonising and infecting multiple body sites including the nasopharynx, lungs, blood, CSF, meninges, and middle ear. We therefore examined 51,379 genomes in the BIGSdb database to determine if there is an association between the presence of *palA* and the isolation site of the strain ("source") (32).

The *palA* gene presence is enriched in carriage isolates and in strains isolated from ear infections compared to strains isolated from IPD or lower respiratory tract disease (Table 2). More than half of serotype 22F and 6A strains isolated from the ear carried *palA* and approximately 28% of all serotype 22F and 6A genomes in the database carry *palA*, in contrast to the overall *palA* prevalence rate of 9.97% (Table 2). By contrast, *palA* was detected in only 6.7% of hypervirulent serotype 1 genomes hosted on the BIGSdb database, and in only 5 of 895 genomes belonging to the multidrug resistant lineage GPSC10 on the Global Pneumococcal Sequencing database (~0.55%). In the BIGSdb database, the only serotype 4 strain isolated from the ear carried *palA* in its genome. These observations suggest that *palA* and/or its putative genetic island may facilitate spread to and cause infection of the ear, although *palA*'s presence is not necessary for colonisation of the ear.

Mutation of *palA* does not alter pneumococcal colonisation or microinvasion of the epithelium. To determine if PalA plays a role in epithelial microinvasion, we generated *palA* deletion and complementation mutants for testing in our NPE model. The deletion and complementation mutants were verified using Sanger sequencing, Illumina sequencing and semi-quantitative PCR of *palA* transcript (Supplementary Table 1, Supplementary Figure 2). Although there is a small reduction in the number of planktonic bacteria, the numbers of epithelial-associated and intracellular BHN418 *palA::kan* were not significantly different to that of WT BHN418 (Figure 5A-C). Additionally, we did not observe a growth defect when BHN418 *palA::kan* was grown in THY or MEM (Figure 5D-E).

Mutation of *lgt* attenuates nasopharyngeal colonisation density and duration in mice (14). We next asked if presence of *palA* confer a survival advantage in a more complex and immune-replete environment such as the murine nasopharynx. Outbred CD-1 female mice were intranasally inoculated with wild-type BHN418 and the *palA* mutant either singly or in a 1:1 competitive mix. After 7 days of colonisation, similar CFU numbers for WT BHN418 and the *palA::kan* were recovered from nasal washes (Figure 5F-G). Similar CFU numbers for BHN418 and *palA::kan* were also recovered in homogenised lungs and blood 24 hours post inoculation in a murine pneumonia model (Figure 5H-I). We conclude that presence of *palA* does not confer a colonisation advantage in the murine nasopharynx or in the progression to bacteraemic pneumonia.

To further probe the function of PalA, we heterologously expressed *palA* in a serotype 23F strain naturally lacking the island (P1121). Semi-quantitative PCR of *palA* transcripts demonstrated substantial *palA* expression driven by the inducible promoter (Supplementary Figure 2C). Expression of *palA* in P1121 did not increase

the microinvasion potential of the resulting strains and reduced the number of planktonic bacteria in the cell culture supernatant (Figure 6A-C). Moreover, the BHN418 *palA* knockout strains and the P1121 *palA* knock-in strains activated TLR2 signalling to similar levels as their respective wild-type strains (Figure 6D). We therefore conclude that presence of *palA* is not solely responsible for the observed strain-specific differences in Lgt-mediated epithelial microinvasion. Moreover, PalA does not contribute significantly to pneumococci's ability to activate TLR2.

DISCUSSION

In this study, we demonstrated that pneumococcal lipoproteins trigger inflammation during epithelial colonisation at least partially via the TLR2-dependent pathway. We have previously shown that epithelial microinvasion can occur in the absence of disease and that there is heightened epithelial inflammation around the time of pneumococcal clearance in controlled human infection (2). In murine models, mutation of *lgt* reduces carriage duration and attenuates disease, associated with a concomitant reduction in inflammatory and immune responses (8, 9, 33). However, although we have shown that BHN418 *lgt::cm* but not TIGR4 *lgt::cm* was significantly attenuated in epithelial adherence and microinvasion compared to their respective wild-type strains, this does not appear to be TLR2-dependent or due to differential lipoprotein repertoires encoded by the strains.

We additionally observed that presence of *lgt* and therefore TLR2 activation heightens the epithelial interferon response elicited by pneumococcal microinvasion in the absence of immune cells. Induction of the interferon pathway upon pneumococcal challenge is thought to be dependent on sensing of intracellular pneumococci, pneumococcal DNA or cellular DNA damage by the infected cells (34–39). In infant mice co-infected with pneumococci and influenzae, interferon signalling increases bacterial shedding while protecting against invasive disease, while TLR2 signalling limits bacterial shedding and transmission (18, 40, 41). Since TLR2 signalling augments the interferon response by human nasopharyngeal epithelial cells during mono-pneumococcal infection, it is unclear how these two pathways mediate the outcomes of pneumococcal microinvasion, colonisation or progression to disease in people. Nonetheless, our results suggest that mucosal innate immunity

could be targeted alongside the induction of an adaptive immune response to prevent pneumococcal colonisation, transmission and invasive disease.

We have implicated lipoprotein expression in intraspecies differences in NPE cell microinvasion but our genetic and mutational analysis lead us to suggest that this is not due to differences in lipoprotein repertoire, but potentially due to differential post-translational lipidation kinetics. The lipoprotein PsaA functions as a bacterial adhesin which binds to host cell E-cadherin (42). In theory, we should have observed a significant reduction in the number of epithelial-associated bacteria for both the TIGR4 and BHN418 *lgt* mutants compared to wild-type due to the loss of PsaA surface presentation; however, our data did not reflect this hypothesis. Similar subtle effects have been seen for example when mutating the lipoprotein encoding gene *dacB* but not *lgt* alters murein sacculus composition, and when mutating *lgt* results in strain-dependent variable effects on growth in rich medium (5, 9, 14, 33, 43). The observation that genetic complementation of *lgt* in BHN418 restores pneumococcal ability to trigger epithelial inflammation and retain PiuA and other lipoproteins in whole cell lysate, but not restore WT levels of microinvasion further suggests that regulation of lipoprotein processing may be more complex than previously thought. The assumption that Lgt and other lipoprotein modification proteins are constitutively expressed and active, and all 30+ lipoproteins are processed at similar rates may not be entirely correct.

We therefore speculate that unlike Gram-negative bacteria, for which lipoprotein processing is essential, pneumococci and other Gram-positive bacteria may compensate for the loss of Lgt by differentially regulating expression of lipoprotein encoding genes, which in turn is regulated by external stimuli in nasopharyngeal niche (44, 45). Proteomics and immunoblotting analyses showed

that abundance of specific lipoproteins increase, decrease or show no change when lipoprotein processing is disrupted in *S. pneumoniae*, although no clear patterns were apparent (5, 13) Additionally, we and others have observed that mutation of *lgt* does not lead to complete loss/release of preprolipoprotein from the cell surface (Supplementary Figure 3) (5). Future investigation into whether pneumococci vary *lgt* expression or Lgt activity to thrive in different tissue niches, in tandem with compensatory regulation of lipoprotein expression, may be warranted. Such a study may reveal novel mechanisms of innate immune evasion. It would also be informative to determine whether there are strain-dependent differences in regulating the generation of TLR2 agonists (mature lipoproteins) and how this may affect the invasiveness and virulence of different pneumococcal lineages.

While investigating the intraspecies variation in the role of *lgt* in microinvasion, we discovered a previously uncharacterised lipoprotein encoding gene (*palA*) and its associated genetic island. Although *palA* presence is enriched in carriage and otitis media isolates, we have not been able to demonstrate a clear role for PalA in epithelial microinvasion, or in a murine model of colonisation or disease. We evaluated bacterial burden in mice 7 days post infection and thus cannot eliminate the possibility that PalA plays a role in the early phases of colonization or in persistence. PalA is predicted by sequence and structure homology to be involved in carbohydrate or sugar transport, although we have yet to identify a substrate for PalA. Raffinose metabolism has been shown to contribute to lung versus ear tropism in serotype 3 and serotype 14 strains (28). It is therefore possible that *palA* functions in promoting niche specialisation by facilitating uptake and metabolism of uncommon sugars, such as raffinose, found in the nasopharynx or middle ear.

In conclusion, we demonstrated a role for pneumococcal surface lipoproteins in triggering epithelial inflammation and augmenting interferon signalling in response to pneumococcal-epithelial interactions. We show that pneumococcal lipoproteins mediate microinvasion in a strain-dependent manner, which may explain the significant attenuation in carriage duration and disease with *lgt* mutants reported by others (8, 14, 33). Additionally, we have characterised a novel accessory lipoprotein likely acquired through horizontal gene transfer but rejected the hypothesis that this lipoprotein contribute to strain differences in pneumococcal epithelial microinvasion. Instead, we postulate that differential regulation of lipoprotein gene expression responding to the nasopharyngeal niche regulate this microinvasion process.

MATERIALS AND METHODS

Bacterial growth and maintenance. *Streptococcus pneumoniae* strains were grown on Columbia agar base with 5% defibrinated horse blood (CBA plates; EO Labs, Oxoid), statically in Todd-Hewitt broth supplemented with 0.5% yeast extract (THY; Oxoid) or in brain heart infusion broth (BHI; Oxoid) at 37°C, 5% CO_2. Where appropriate, growth medium was supplemented with antibiotics at the following concentrations: chloramphenicol (10 µg/ml), erythromycin (0.5 µg/ml), kanamycin (250 µg/ml). Working stocks for infections were prepared by freezing THY cultures at OD_{600} 0.3-0.4 with 10% glycerol. NEB® Stable competent *Escherichia coli* derived strains were grown in LB broth or LB agar (Difco) supplemented with ampicillin (200 µg/ml) where appropriate. Bacterial strains used in this paper are listed in Table 3.

Bacterial genetic manipulation. *S. pneumoniae* were genetically manipulated using a competence stimulating peptide (CSP)-mediated transformation assay (46). Briefly, pneumococci were grown in THY pH 6.8 supplemented with 1 mM $CaCl_2$ and 0.02% BSA at 37°C, 5% CO_2 to OD_{600} 0.01- 0.03, pelleted and resuspended in 1/12 volume THY pH 8.0 supplemented with 1 mM $CaCl_2$ and 0.2% BSA. A total of 400 ng CSP (Cambridge Biosciences; CSP-2 for TIGR4; 1:1 ratio of CSP-1:CSP-2 for BHN418; CSP-1 for P1121) was added to the bacterial suspension and incubated at RT for 5 mins. The suspensions were then mixed with ~300 ng transforming DNA, incubated at 37°C, 5% CO_2 for two hours and plated on CBA plates supplemented with relevant antibiotics. Antibiotic resistant transformants were screened using colony PCR and confirmed by sequencing.

Transforming DNA for generating *lgt::cm* and *palA::kan* mutants were generated using overlap-extension PCR. Complementation and expression constructs were generated by inserting the target gene into the complementation plasmid pASR103 or pPEPY (47), which allows for integration of the construct at a chromosomal ectopic site. Plasmids used are listed in Table 3, while primers are listed in Supplementary Table 3.

Cell culture. Detroit 562 (ATCC® CCL-138™; human pharyngeal carcinoma epithelial cells) were expanded and maintained in MEMα (Gibco™ 22561021) supplemented with 10% heat-inactivated FBS (HI-FBS; LabTech FB-1001/500 or Gibco 10438-026) at 37°C, 5% CO_2. HEK-Blue™ hTLR2 reporter cells (Invivogen, hkb-htlr2) were expanded and maintained in DMEM (4.5 g/L glucose, 2mM glutamine, sodium pyruvate) supplemented with 10% HI-FBS at 37°C, 5% CO_2. Per manufacturer's instructions, DMEM growth medium was supplemented with 100 µg/ml normocin™ and/or 1X HEK-Blue™ Selection (Invivogen) where appropriate.

NPE infections. Adherence-invasion infections of confluent Detroit 562 cells with *S. pneumoniae* strains were performed at MOI 20 (P1121/23F derived strains) or MOI 10 (all others) for 3 hours. Working bacterial stocks were thawed, centrifuged to remove freezing medium and resuspended in infection medium (MEMα with 1% HI-FBS) to the appropriate CFU. 1 ml bacterial suspension were added to each well containing confluent Detroit 562 cells. Plates were incubated statically at 37°C, 5% CO_2 for 3 hours, after which 10 µl of the supernatant were removed for CFU enumeration. For adherence assays, cells were washed thrice with PBS, lysed with cold 1% saponin (10 min incubation at 37°C, followed by vigorous pipetting), and 10

445 µl cell lysate removed for CFU enumeration. For invasion assays, cells were washed
446 thrice with PBS, incubated with 0.5 ml infection medium supplemented with 200
447 µg/ml gentamicin at 37°C, 5% CO_2 for 1 hour to kill extracellular bacteria, followed by
448 3x PBS wash, lysis with 1% saponin and CFU enumeration. Experiments were
449 performed at least thrice on different days ($n \geq 3$ biological replicates) with technical
450 duplicates. Statistical significance was determined using one-way ANOVA with
451 Bonferroni's multiple comparison test.
452
453 To harvest RNA for qPCR, confluent Detroit 562 cells were treated with synthetic
454 agonists or infected with *S. pneumoniae* strains at MOI 10 for 6 hours. Briefly,
455 working bacterial stocks were thawed, centrifuged to remove freezing medium and
456 resuspended in infection medium (MEMα with 1% HI-FBS) to the appropriate CFU.
457 Bacterial suspensions, infection medium (negative control), or infection medium
458 supplemented with synthetic agonists (20 µg/ml Poly(I:C)) (TLR3 agonist, Bio-
459 Techne) were added to each flask. Flasks were incubated statically at 37°C, 5% CO_2
460 for 6 hours, after which 10 µl were removed for CFU enumeration. Detroit 562 cells
461 were washed thrice with PBS and harvested by scraping into 300 µl RNA*later*
462 (ThermoFisher). For each treatment condition, RNA harvesting was performed at
463 least thrice on different days ($n \geq 3$ biological replicates) without technical replicates.
464
465 For growth curve experiments, *S. pneumoniae* strains were seeded into 1 ml THY or
466 1 ml infection medium (MEMα with 1% HI-FBS, LabTech) with and without confluent
467 Detroit 562 cells in 12-well plates at a similar CFU number as used in infection
468 experiments. Plates were incubated at 37°C, 5% CO_2 for 7 hours, with aliquots taken
469 for CFU enumeration every hour. CFU growth curves were performed at least thrice

on different days (n≥3 biological replicates) without technical replicates. Statistical significance was determined using Student's *t*-test assuming equal variance.

Quantitiative and semi-quantitative PCR. RNA from epithelial cells stored in RNA*later* were extracted using RNeasy Mini kit (Qiagen) according to manufacturer instructions. Carryover DNA was removed with TURBO DNA-*free* kit (Ambion), and cDNA generated using LunaScript® RT Supermix kit (NEB). qPCR was performed using Luna® Universal qPCR Master Mix (NEB) in technical triplicates with primers specific for *GAPDH*, *CXCL10*, *IFNB1*, *IFNL1,* and *IFNL3* (Supplementary Table 3). Whenever possible qPCR primers were designed to span exon-exon junctions. Cycling conditions are as follows: 95°C for 5 mins, 40 cycles of 95°C for 15 secs and 60.5°C for 45 secs, with a plate read at the end of each cycle. Data was analysed using the $2^{\Delta\Delta Ct}$ method, with media only control and *GAPDH* levels for normalization. Statistical significance was determined using Student's *t*-test assuming equal variance.

RNA from *S. pneumoniae* stored in RNA*later* were extracted using a modified TRIzol™ (Ambion) protoocol. Briefly, pneumococcal strains were grown in BHI to OD_{600} ~0.5, harvested by centrifugation at 8.000 x *g* for 8 mins, resuspended in 300 µl RNA*later* and saved at -70°C. On the extraction day, the suspensions were thawed, subjected to centrifugation at 8.000 x *g* for 8 mins, followed by removal of RNA*later* and resuspension of the bacterial pellet in 1ml TRIzol™ reagent. The whole 1ml suspension was transferred to pre-chilled VK01 Precellys® lysing tubes containing glass beads (Stretton Scientific) and subjected to lysis by bead beating (Precellys® Evolution; 6,200 RPM, 4 x 45 secs cycles with 20 secs rest in between

cycle). The TRIzol™ lysates were then centrifuged at 5, 000 x *g* for 10 mins at 4°C, and ~ 800 µl supernatant transferred to a new, pre-chilled centrifuge tube. RNA extraction and cDNA generation were performed as described above. Semi-quantitative PCR was performed using OneTaq® Quick-Load® Master Mix (NEB) using primers against *lgt, palA* and 16s rRNA with cycling conditions: 95°C for 5 mins, 40 cycles of 95°C for 15 secs and 60.5°C for 45 secs. Amplification products were analyzed using DNA gel electrophoresis.

Immunoblotting. 5ml cultures of pneumococcal strains grown in BHI to OD ~0.5 were harvested by centrifugation at 3,900 x *g* for 15 mins, resuspended in 1 ml 1X PBS with 0.1% NP-40 and transferred into pre-chilled VK01 Precellys® lysing tubes containing glass beads (Stretton Scientific). Pneumococcal suspensions were lysed by bead beating (Precellys® Evolution; 6,200 RPM, 4 x 45 secs cycles with 20 secs rest in between cycle), followed by centrifugation at 5, 000 x *g* for 10 mins at 4°C to pellet debris. Approximately 800 µl supernatant (whole cell lysates) were transferred to a fresh centrifuge tube and saved at -70°C until further use. Protein concentration was determined using Bradford reagent (Thermo Scientific) per manufacturer's instructions and used to normalize the amount of whole cell lysate used in immunoblotting. Lysates were mixed with loading buffer, incubated at 70°C for 10 mins, and chilled on ice prior to gel loading.

Approximately 3.5 µg and 2 µg whole cell lysate were loaded on NuPage™ 4-12% Bis-Tris protein gels (Invitrogen) and subjected to gel electrophoresis and transferred onto nitrocellulose membranes. Membranes were blocked in 1X TBS pH 7.4 with 0.05% Tween-20 and 5% skim milk (hereafter blocking buffer) at RT for 1 hour,

520 washed thrice in 1X TBS pH 7.4 with 0.05% Tween-20 (wash buffer; 5 mins
521 incubation at RT per wash) and probed with antisera from mice inoculated with
522 polysaccharide conjugated-PiuA (1:1,000) or human intravenous immunoglobulin
523 (IVIG; 1:1,000) (Vigam® Liquid) in blocking buffer overnight at 4°C (48). Membranes
524 were washed thrice, incubated with IRDye 800W-conjugated polyclonal goat α-
525 mouse or goat α-human antibody in blocking buffer (1:10.000) (Abcam) at RT for 1
526 hour, washed thrice and imaged using LiCor Odyssey CLx. Equal loading was
527 checked using PonceauS staining.
528
529 **HEK-Blue hTLR2 reporter assay.** HEK-Blue™ hTLR2 secreted alkaline
530 phosphatase (SEAP) reporter assays were performed according to manufacturer
531 instructions (Invivogen, hkb-htlr2). Briefly, HEK-Blue™ hTLR2 cells, *S. pneumoniae*
532 and control reagents were resuspended or diluted in pre-warmed HEK-Blue™
533 Detection medium (Invivogen). 5 x 10^4 HEK-Blue™ hTLR2 cells were mixed with 5 x
534 10^5 CFU *S. pneumoniae* (MOI 10) and incubated for 16 hours at 37°C, 5% CO_2.
535 SEAP activity was then measured spectroscopically at A_{620}. 100 ng/ml of Pam_2CSK_4
536 and Pam_3CSK_4 (TLR2 agonist, Bio-Techne) were used as positive controls, while
537 bacterial-free medium was used as negative control. Experiments were performed at
538 least thrice on different days ($n \geq 3$ biological replicates) with technical triplicates.
539 Statistical significance was determined using one-way ANOVA with Bonferroni's
540 multiple comparison test.
541
542 **Lipoprotein prediction using MEME suite.** Amino acid sequences of thirty-nine
543 published D39 lipoproteins were used with the motif discovery tool MEME to identify
544 pneumococcal lipoprotein motif(s) (5, 13, 22). The top two MEME results were

545 combined to obtain motif: L[LA][AS][AL]LXL[AV]A**C**[SG][NQS], a modified extension
546 of the minimal lipobox motif LAG**C** (5).
547
548 The obtained motif was used with the motif scanning tool FIMO to identify
549 lipoproteins in the genomes of *S. pneumoniae* TIGR4, BHN418 and D39, with the
550 latter used for quality control (49). Match *p*-value was set to 0.001. FIMO results
551 were further filtered with the following criteria: (i) presence of the lipidated cysteine
552 residue in the motif, (ii) presence of motif in the first 70 a.a. of the sequence, iii)
553 positive prediction as lipoprotein by SignalP-6.0 (50).
554
555 **Genomic analysis.** Presence of *palA* and its associated genetic island were
556 determined using Local-BLAST (BLASTN, TBLASTN) for the Malawian carriage
557 dataset (n=51,379) and serotype 23F strain P1121 (51). The built-in BLAST tool on
558 pubmlst.org was used for analysis of the BIGSdb dataset (32). BLASTN and
559 TBLASTN tools on the NCBI database were used to identify *palA* and PalA
560 homologues in non-pneumococcal species (51, 52). BLAST results were exported in
561 csv format and further analysed using R (v3.6.0) in RStudio
562 (http://www.rstudio.com/). Presence/absence of *palA* was annotated onto a Newick
563 tree showing phylogeny of the Malawian carriage strains by metabolic type and
564 visualized using iTOL (53, 54). Potential gene functions were inferred through the
565 results of BLASTP and NCBI Conserved Domain Database searches (51, 52, 55).
566
567 The BHN418 genome assembly was generated by combining long read sequencing
568 (PacBio) and short read sequencing (Illumina) methods which resulted in a single
569 contiguous chromosome of BHN418 of length 2,107,426 bp. *De novo* assembly was

performing using the Unicycler v0.4.8 pipeline in bold mode, quality assessed using QUAST v5.1.0rc1 and annotated using Bakta v1.8.2 as described previously (56–59). TIGR4 sequencing reads were aligned to the BHN418 genome using Samtools v1.14 and visualised using IGV v2.16.1 (29, 52).

Genomes of TIGR4 and/or BHN418 *lgt::cm*, *palA::kan* and respective complementation strains were assembled *de novo* using SPAdes 3.15.5 with standard parameters, and subjected to Local-BLAST (TBLASTN) to determine the presence or absence of *lgt*, *palA, cm* and *kan* in the respective genomes (52, 60).

TLR2 transcriptional module analysis. TLR2-mediated transcriptional activity in Detroit 562 cells infected with TIGR4 and BHN418 for 3 hours were determined using published RNAseq data (2). We generated a transcriptional module reflective of TLR2 activity derived from genes overexpressed in fibroblasts stimulated with TLR2 agonists Pam_2CSK_4 and/or FSL-1 for 6 hours relative to unstimulated controls (>1.5 fold; paired *t*-test with α of $p<0.05$ without multiple testing correction) (Gene Expression Omnibus (GEO) dataset GSE92466) (Supplementary Figure 1A) (19). Module expression was determined by calculating the geometric mean expression of all constituent genes found in the analysed RNAseq dataset. Performance was validated using data derived from Acute Myeloid Leukemia cells (GEO datasets GSE92744) and CD14+ monocytes stimulated with Pam_3CSK_4 (GEO dataset GSE78699) (Supplementary Figure 1B-C) (61, 62).

Murine experiments. Outbred female CD1 mice (Charles River Laboratories) were inoculated intranasally under anaesthetic (isoflurane) with 1×10^7 CFU bacteria (n=6

for single inoculation colonisation and pneumonia model, n=7 for competition experiment). For colonisation experiments, nasal washes were performed 7 days post infection using 1 ml PBS. For pneumonia model, mice were sacrificed 24 hpi and bacteria recovered from the blood and homogenized lungs. CFU numbers were enumerated using CBA supplemented with 4 µg/ml gentamicin, with additional 250 µg/ml kanamycin where appropriate. All animal procedures were approved by the local ethical review process and conducted in accordance with the relevant UK Home Office approved project license (PPL70/6510). Mice were housed for at least one week under standard conditions before use. Randomisation or blinding was not performed for these experiments. Statistical significance was determined using Mann-Whitney test.

Data availability. BHN418, ECSPN100, ECSPN106, ECSPN200, ECSPN210, ECSPN211 and ECSPN213 genomes were deposited to NCBI with BioProject accession number PRJNA1022026 (BHN418) and PRJNA1087740 (everything else). TIGR4 sequencing reads were downloaded from NCBI Sequence Reads Archive (accession SRX6259281), while P1121 reads were downloaded from the EMBL-EBI database (accession ERS1072059) (63, 64). D39 and TIGR4 whole genome assemblies were downloaded from NCBI GenBank database (accession numbers CP000410.2 and AE005672.3, respectively) (65). All other genomic sequences used were hosted on the PubMLST Pneumococcal Genome Library (https://pubmlst.org/organisms/streptococcus-pneumoniae/pgl) or the Global Pneumococcal Sequencing project database (https://www.pneumogen.net/gps/) (32, 53). RNAseq data used in the TLR2 transcriptional module expression analysis were obtained from the ArrayExpress database (accession E-MTAB-7841) (6).

620

ACKNOWLEDGEMENTS

We would like to thank A. Gori and CJ Yang for bioinformatics support and the Jolly, Tomlinson, and Towers groups at UCL for sharing supplies and equipment. This study was funded by a Medical Research Council grant (MR/T016329/1) awarded to RSH and JSB which supported JMC and CMW. JMC and MB were also supported by funding from NIHR Global Health Research Unit on Mucosal Pathogens at UCL, commissioned by the National Institute for Health Research using Official Development Assistance (ODA) funding. GP is supported by funding from the UCLH NIHR Biomedical Research Centre. RSH is a NIHR Senior Investigator. The views expressed are those of the authors and not necessarily those of the NIHR.

REFERENCES

1. Weiser JN, Ferreira DM, Paton JC. 2018. *Streptococcus pneumoniae*: Transmission, colonization and invasion. Nat Rev Microbiol 16:355–367.
2. Weight CM, Venturini C, Pojar S, Jochems SP, Reiné J, Nikolaou E, Solórzano C, Noursadeghi M, Brown JS, Ferreira DM, Heyderman RS. 2019. Microinvasion by *Streptococcus pneumoniae* induces epithelial innate immunity during colonisation at the human mucosal surface. Nat Commun 10:3060.
3. Jochems SP, de Ruiter K, Solórzano C, Voskamp A, Mitsi E, Nikolaou E, Carniel BF, Pojar S, German EL, Reiné J, Soares-Schanoski A, Hill H, Robinson R, Hyder-Wright AD, Weight CM, Durrenberger PF, Heyderman RS, Gordon SB, Smits HH, Urban BC, Rylance J, Collins AM, Wilkie MD, Lazarova L, Leong SC, Yazdanbakhsh M, Ferreira DM. 2019. Innate and adaptive nasal mucosal immune responses following experimental human pneumococcal colonization. J Clin Invest 129:4523–4538.
4. Trimble A, Connor V, Robinson RE, McLenaghan D, Hancock CA, Wang D, Gordon SB, Ferreira DM, Wright AD, Collins AM. 2020. Pneumococcal colonisation is an asymptomatic event in healthy adults using an experimental human colonisation model. PLoS One 15:e0229558.
5. Kohler S, Voß F, Gómez Mejia A, Brown JS, Hammerschmidt S. 2016. Pneumococcal lipoproteins involved in bacterial fitness, virulence, and immune evasion. FEBS Lett 590:3820–3839.
6. Mitchell AM, Mitchell TJ. 2010. *Streptococcus pneumoniae*: Virulence factors and variation. Clin Microbiol Infect 16:411–418.

7. Moffitt K, Howard A, Martin S, Cheung E, Herd M, Basset A, Malley R. 2015. Th17-mediated protection against pneumococcal carriage by a whole-cell vaccine is dependent on Toll-like receptor 2 and surface lipoproteins. Clin Vaccine Immunol 22:909–916.
8. Jang A-Y, Ahn KB, Zhi Y, Ji H, Zhang J, Han SH, Guo H, Lim S, Song JY, Lim JH, Seo HS. 2019. Serotype-independent protection against invasive pneumococcal infections conferred by live vaccine with *lgt* deletion. Front Immunol 10:1212.
9. Tomlinson G, Chimalapati S, Pollard T, Lapp T, Cohen J, Camberlein E, Stafford S, Periselneris J, Aldridge C, Vollmer W, Picard C, Casanova J-L, Noursadeghi M, Brown J. 2020. TLR-mediated inflammatory responses to *Streptococcus pneumoniae* are highly dependent on surface expression of bacterial lipoproteins. J Immunol 193:3736–3745.
10. Barendt SM, Sham L, Winkler ME. 2011. Characterization of mutants deficient in the L,D -Carboxypeptidase (DacB) and WalRK (VicRK) regulon, involved in peptidoglycan maturation of *Streptococcus pneumoniae* serotype 2 strain D39. J Bacteriol 193:2290–2300.
11. Russell H, Tharpe JA, Wells DE, White EH, Johnson JE. 1990. Monoclonal antibody recognizing a species-specific protein from *Streptococcus pneumoniae*. J Clin Microbiol 28:2191–2195.
12. Lawrence MC, Pilling PA, Epa VC, Berry AM, Ogunniyi AD, Paton JC. 1998. The crystal structure of pneumococcal surface antigen PsaA reveals a metal-binding site and a novel structure for a putative ABC-type binding protein. Curr Biol 6:1553–1561.
13. Pribyl T, Moche M, Dreisbach A, Bijlsma JJE, Saleh M, Abdullah MR, Hecker

M, van Dijl JM, Becher D, Hammerschmidt S. 2014. Influence of impaired lipoprotein biogenesis on surface and exoproteome of *Streptococcus pneumoniae*. J Proteome Res 13:650–667.

14. Chimalapati S, Cohen JM, Camberlein E, MacDonald N, Durmort C, Vernet T, Hermans PWM, Mitchell T, Brown JS. 2012. Effects of deletion of the *Streptococcus pneumoniae* lipoprotein diacylglyceryl transferase gene *lgt* on ABC transporter function and on growth *in vivo*. PLoS One 7:e41393.

15. Aaberge IS, Eng J, Lermark G, Løvik M. 1995. Virulence of Streptococcus pneumoniae in mice: a standardized method for preparation and frozen storage of the experimental bacterial inoculum. Microb Pathog 18:141–152.

16. Browall S, Norman M, Tångrot J, Galanis I, Sjöström K, Dagerhamn J, Hellberg C, Pathak A, Spadafina T, Sandgren A, Bättig P, Franzén O, Andersson B, Örtqvist Å, Normark S, Henriques-Normark B. 2014. Intraclonal variations among *Streptococcus pneumoniae* isolates influence the likelihood of invasive disease in children. J Infect Dis 209:377–388.

17. Sleeman KL, Griffiths D, Shackley F, Diggle L, Gupta S, Maiden MC, Moxon ER, Crook DW, Peto TEA. 2006. Capsular serotype-specific attack rates and duration of carriage of *Streptococcus pneumoniae* in a population of children. J Infect Dis 194:682–688.

18. Richard AL, Siegel SJ, Erikson J, Weiser JN. 2014. TLR2 signaling decreases transmission of Streptococcus pneumoniae by limiting bacterial shedding in an infant mouse Influenza A co-infection model. PLoS Pathog 10:e1004339.

19. Della Mina E, Borghesi A, Zhou H, Bougarn S, Boughorbel S, Israel L, Meloni I, Chrabieh M, Ling Y, Itan Y, Renieri A, Mazzucchelli I, Basso S, Pavone P, Falsaperla R, Ciccone R, Cerbo RM, Stronati M, Picard C, Zuffardi O, Abel L,

Chaussabel D, Marr N, Li X, Casanova J-L, Puel A. 2017. Inherited human IRAK-1 deficiency selectively impairs TLR signaling in fibroblasts. Proc Natl Acad Sci 114:E514–E523.

20. Lee KS, Scanga CA, Bachelder EM, Chen Q, Snapper CM. 2007. TLR2 synergizes with both TLR4 and TLR9 for induction of the MyD88-dependent splenic cytokine and chemokine response to *Streptococcus pneumoniae*. Cell Immunol 245:103–110.

21. Dessing MC, Hirst RA, de Vos AF, van der Poll T. 2009. Role of Toll-like receptors 2 and 4 in pulmonary inflammation and injury induced by pneumolysin in mice. PLoS One 4:e7993.

22. Bailey TL, Johnson J, Grant CE, Noble WS. 2015. The MEME Suite. Nucleic Acids Res 43:W39–W49.

23. Dwyer MA, Hellinga HW. 2004. Periplasmic binding proteins: a versatile superfamily for protein engineering. Curr Opin Struct Biol 14:495–504.

24. Kelley LA, Mezulis S, Yates CM, Wass MN, Sternberg MJE. 2015. The Phyre2 web portal for protein modelling, prediction, and analysis. Nat Protoc 10:845–858.

25. Jumper J, Evans R, Pritzel A, Green T, Figurnov M, Ronneberger O, Tunyasuvunakool K, Bates R, Žídek A, Potapenko A, Bridgland A, Meyer C, Kohl SAA, Ballard AJ, Cowie A, Romera-Paredes B, Nikolov S, Jain R, Adler J, Back T, Petersen S, Reiman D, Clancy E, Zielinski M, Steinegger M, Pacholska M, Berghammer T, Bodenstein S, Silver D, Vinyals O, Senior AW, Kavukcuoglu K, Kohli P, Hassabis D. 2021. Highly accurate protein structure prediction with AlphaFold. Nature 596:583–589.

26. Wilkens S. 2015. Structure and mechanism of ABC transporters. F1000Prime

Rep 7:14.

27. Rosenow C, Maniar M, Trias J. 1999. Regulation of the alpha-galactosidase activity in *Streptococcus pneumoniae*: Characterization of the raffinose utilization system. Genome Res 9:1189–1197.

28. Minhas V, Harvey RM, McAllister LJ, Seemann T, Syme AE, Baines SL, Paton JC, Trappetti C. 2019. Capacity to utilize raffinose dictates pneumococcal disease phenotype. MBio 10:e02596-18.

29. Tettelin H, Nelson KE, Paulsen IT, Eisen JA, Read TD, Peterson S, Heidelberg J, DeBoy RT, Haft DH, Dodson RJ, Durkin AS, Gwinn M, Kolonay JF, Nelson WC, Peterson JD, Umayam LA, White O, Salzberg SL, Lewis MR, Radune D, Holtzapple E, Khouri H, Wolf A le. M, Utterback TR, Hansen CL, McDonald LA, Feldblyum T V., Angiuoli S, Dickinson T, Hickey EK, Holt IE, Loftus BJ, Yang F, Smith HO, Venter JC, Dougherty BA, Morrison DA, Hollingshead SK, Fraser CM. 2001. Complete genome sequence of a virulent isolate of *Streptococcus pneumoniae*. Science (80-) 293:498–506.

30. Spellerberg B, Cundell DR, Sandros J, Pearce BJ, Idänpään-Heikkilä I, Rosenow C, Masure HR. 1996. Pyruvate oxidase, as a determinant of virulence in Streptococcus pneumoniae. Mol Microbiol 19:803–813.

31. Obolski U, Swarthout TD, Kalizang'oma A, Mwalukomo TS, Chan JM, Weight CM, Brown C, Cave R, Cornick J, Kamng'ona AW, Msefula J, Ercoli G, Brown JS, Lourenço J, Maiden MC, French N, Gupta S, Heyderman RS. 2023. The metabolic, virulence and antimicrobial resistance profiles of colonising *Streptococcus pneumoniae* shift after PCV13 introduction in urban Malawi. Nat Commun 14:7477.

32. Jolley KA, Maiden MCJ. 2010. BIGSdb: Scalable analysis of bacterial genome

757 variation at the population level. BMC Bioinformatics 11:595.
758 33. Petit CM, Brown JR, Ingraham K, Bryant AP, Holmes DJ. 2001. Lipid
759 modification of prelipoproteins is dispensable for growth *in vitro* but essential
760 for virulence in *Streptococcus pneumoniae*. FEMS Microbiol Lett 200:229–233.
761 34. Joyce EA, Popper SJ, Falkow S. 2009. *Streptococcus pneumoniae*
762 nasopharyngeal colonization induces type I interferons and interferon-induced
763 gene expression. BMC Genomics 10:404.
764 35. Skovbjerg S, Nordén R, Martner A, Samuelsson E, Hynsjö L, Wold AE. 2017.
765 Intact pneumococci trigger transcription of interferon-related genes in human
766 moncytes, while fragmented, autolyzed bacteria subvert this response. Infect
767 Immun 85:e00960-16.
768 36. Parker D, Martin FJ, Soong G, Harfenist BS, Aguilar JL, Ratner AJ, Fitzgerald
769 KA, Schindler C, Prince A. 2011. *Streptococcus pneumoniae* DNA initiates
770 type I interferon signaling in the respiratory tract. MBio 2:e00016-11.
771 37. D'Mello A, Riegler AN, Martínez E, Beno SM, Ricketts TD, Foxman EF,
772 Orihuela CJ, Tettelin H. 2020. An in vivo atlas of host–pathogen
773 transcriptomes during *Streptococcus pneumoniae* colonization and disease.
774 Proc Natl Acad Sci U S A 117:33507–33518.
775 38. Koppe U, Högner K, Doehn J-M, Müller HC, Witzenrath M, Gutbier B, Bauer S,
776 Pribyl T, Hammerschmidt S, Lohmeyer J, Suttorp N, Herold S, Opitz B. 2012.
777 *Streptococcus pneumoniae* stimulate a STING- and IFN regulatory factor 3-
778 dependent type I IFN production in macrophages, which regulates RANTES
779 production in macrophages, cocultured alveolar epithelial cells, and mouse
780 lungs. J Immunol 188:811–817.
781 39. Ruiz-Moreno JS, Hamann L, Jin L, Sander LE, Puzianowska-Kuznicka M,

Cambier J, Witzenrath M, Schumann RR, Suttorp N, Opitz B, Group CS. 2018. The cGAS/STING pathway detects *Streptococcus pneumoniae* but appears dispensable for antipneumococcal defense in mice and humans. Infect Immun 86:e00849-17.

40. LeMessurier KS, Häcker H, Chi L, Tuomanen E, Redecke V. 2013. Type I interferon protects against pneumococcal invasive disease by inhibiting bacterial transmigration across the lung. PLoS Pathog 9:e1003727.

41. Zangari T, Ortigoza MB, Lokken-Toyli KL, Weiser JN. 2021. Type I interferon signaling is a common factor driving *Streptococcus pneumoniae* and Influenza A virus shedding and transmission. MBio 12:e03589-20.

42. Anderton JM, Rajam G, Romero-Steiner S, Summer S, Kowalczyk AP, Carlone GM, Sampson JS, Ades EW. 2007. E-cadherin is a receptor for the common protein pneumococcal surface adhesin A (PsaA) of Streptococcus pneumoniae. Microb Pathog 42:225–236.

43. Abdullah MR, Gutiérrez-Fernández J, Pribyl T, Gisch N, Saleh M, Rohde M, Petruschka L, Burchhardt G, Schwudke D, Hermoso JA, Hammerschmidt S. 2014. Structure of the pneumococcal L,D-carboxypeptidase DacB and pathophysiological effects of disabled cell wall hydrolases DacA and DacB. Mol Microbiol 93:1183–1206.

44. Smithers L, Olatunji S, Caffrey M. 2021. Bacterial Lipoprotein Posttranslational Modifications. New Insights and Opportunities for Antibiotic and Vaccine Development. Front Microbiol 12:788445.

45. Nguyen MT, Matsuo M, Niemann S, Herrmann M, Götz F. 2020. Lipoproteins in Gram-Positive Bacteria: Abundance, Function, Fitness. Front Microbiol 11:582582.

46. Zhu L, Lau GW. 2011. Inhibition of competence development, horizontal gene transfer and virulence in Streptococcus pneumoniae by a modified competence stimulating peptide. PLoS Pathog 7:e1002241.
47. Keller LE, Robinson DA, McDaniel LS. 2016. Nonencapsulated *Streptococcus pneumoniae*: Emergence and pathogenesis. MBio 7:e01792-15.
48. Reglinski M, Ercoli G, Plumptre C, Kay E, Petersen FC, Paton JC, Wren BW, Brown JS. 2018. A recombinant conjugated pneumococcal vaccine that protects against murine infections with a similar efficacy to Prevnar-13. npj Vaccines 3:53.
49. Grant CE, Bailey TL, Noble WS. 2011. FIMO: scanning for occurrences of a given motif. Bioinformatics 27:1017–1018.
50. Teufel F, Almagro Armenteros JJ, Johansen AR, Gíslason MH, Pihl SI, Tsirigos KD, Winther O, Brunak S, von Heijne G, Nielsen H. 2022. SignalP 6.0 predicts all five types of signal peptides using protein language models. Nat Biotechnol 40:1023–1025.
51. Altschul SF, Madden TL, Schäffer AA, Zhang J, Zhang Z, Miller W, Lipman DJ. 1997. Gapped BLAST and PSI-BLAST: a new generation of protein database search programs. Nucleic Acids Res 25:3389–3402.
52. Sayers EW, Barrett T, Benson DA, Bryant SH, Canese K, Chetvernin. V, Church DM, Dicuccio M, Edgar R, Federhen S, Feolo M, Geer LY, Helmberg W, Kapustin Y, Landsman D, Lipman DJ, Madden TL, Maglott DR, Miller V, Mizrachi I, Ostell J, Pruitt KD, Schuler GD, Sequeira E, Sherry ST, Shumway M, Sirotkin K, Souvorov A, Starchenko G, Tatusova TA, Wagner L, Yaschenko E, Ye J. 2009. Database resources of the National Center for Biotechnology Information. Nucleic Acids Res 37:5–15.

53. Gori A, Obolski U, Swarthout TD, Lourenço J, Weight CM, Cornick J, Kamng'ona A, Mwalukomo TS, Msefula J, Brown C, Maiden MC, French N, Gupta S, Heyderman RS. 2021. The metabolic, virulence and antimicrobial resistance profiles of colonizing Streptococcus pneumoniae shift after pneumococcal vaccine introduction in urban Malawi. medRxiv 2021.07.21.21260914.
54. Letunic I, Bork P. 2021. Interactive tree of life (iTOL) v5: An online tool for phylogenetic tree display and annotation. Nucleic Acids Res 49:W293–W296.
55. Machler-Bauer A, Bo Y, Han L, He J, Lanczycki C, Lu S, Chitsaz F, Derbyshire M, Geer R, Gonzales N, Gwadz M, Hurwitz D, Lu F, Machler G, Song J, Thanki N, Wang Z, Yamashita R, Zhang D, Zheng C, Geer L, Bryant S. 2017. CDD/SPARCLE: functional classification of proteins via subfamily domain architectures. Nucleic Acids Res 45:D200–D203.
56. Wick RR, Judd LM, Gorrie CL, Holt KE. 2017. Unicycler: Resolving bacterial genome assemblies from short and long sequencing reads. PLOS Comput Biol 13:e1005595.
57. Gurevich A, Saveliev V, Vyahhi N, Tesler G. 2013. QUAST: quality assessment tool for genome assemblies. Bioinformatics 29:1072–1075.
58. Betts M, Jarvis S, Jeffries A, Gori A, Chaguza C, Msefula J, Weight CM, Kwambana-Adams B, French N, Swarthout TD, Brown JS, Heyderman RS. 2021. Complete Genome Sequence of Streptococcus pneumoniae Strain BVJ1JL, a Serotype 1 Carriage Isolate from Malawi. Microbiol Resour Announc 10:10.1128/mra.00715-21.
59. Schwengers O, Jelonek L, Dieckmann MA, Beyvers S, Blom J, Goesmann A. 2021. Bakta: Rapid and standardized annotation of bacterial genomes via

alignment-free sequence identification. Microb Genomics 7:000685.

60. Prjibelski A, Antipov D, Meleshko D, Lapidus A, Korobeynikov A. 2020. Using SPAdes De Novo Assembler. Curr Protoc Bioinforma 70:e102.

61. Lachmandas E, Boutens L, Ratter JM, Hijmans A, Hooiveld GJ, Joosten LAB, Rodenburg RJ, Fransen JAM, Houtkooper RH, van Crevel R, Netea MG, Stienstra R. 2016. Microbial stimulation of different Toll-like receptor signalling pathways induces diverse metabolic programmes in human monocytes. Nat Microbiol 2:16246.

62. Eriksson M, Peña-Martínez P, Ramakrishnan R, Chapellier M, Högberg C, Glowacki G, Orsmark-Pietras C, Velasco-Hernández T, Lazarević VL, Juliusson G, Cammenga J, Mulloy JC, Richter J, Fioretos T, Ebert BL, Järås M. 2017. Agonistic targeting of TLR1/TLR2 induces p38 MAPK-dependent apoptosis and NFκB-dependent differentiation of AML cells. Blood Adv 1:2046–2057.

63. Tettelin H, Masignani V, Cieslewicz MJ, Donati C, Medini D, Ward NL, Angiuoli S V, Crabtree J, Jones AL, Durkin AS, Deboy RT, Davidsen TM, Mora M, Scarselli M, Ros IM y, Peterson JD, Hauser CR, Sundaram JP, Nelson WC, Madupu R, Brinkac LM, Dodson RJ, Rosovitz MJ, Sullivan SA, Daugherty SC, Haft DH, Selengut J, Gwinn ML, Zhou L, Zafar N, Khouri H, Radune D, Dimitrov G, Watkins K, O'Connor KJB, Smith S, Utterback TR, White O, Rubens CE, Grandi G, Madoff LC, Kasper DL, Telford JL, Wessels MR, Rappuoli R, Fraser CM. 2005. Genome analysis of multiple pathogenic isolates of *Streptococcus agalactiae*: Implications for the microbial "pan-genome." Proc Natl Acad Sci U S A 102:13950–13955.

64. Pojar S, Basset A, Gritzfeld JF, Nikolaou E, Selm S van, Eleveld MJ,

Gladstone RA, Solórzano C, Dalia AB, German E, Mitsi E, Connor V, Hyder-Wright AD, Hill H, Hales C, Chen T, Camilli A, Collins AM, Rylance J, Bentley SD, Jochems SP, Jonge MI de, Weiser JN, Cleary DW, Clarke S, Malley R, Gordon SB, Ferreira DM. 2020. Isolate differences in colonization efficiency during experimental human pneumococcal challenge. medRxiv 2020.04.20.20066399.

65. Lanie JA, Ng W-L, Kazmierczak KM, Andrzejewski TM, Davidsen TM, Wayne KJ, Hervé T, Glass JI, Winkler ME. 2007. Genome Sequence of Avery's Virulent Serotype 2 Strain D39 of Streptococcus pneumoniae and Comparison with That of Unencapsulated Laboratory Strain R6. J Bacteriol 189:38–51.

66. Khandavilli S, Homer KA, Yuste J, Basavanna S, Mitchell T, Brown JS. 2008. Maturation of *Streptococcus pneumoniae* lipoproteins by a type II signal peptidase is required for ABC transporter function and full virulence. Mol Microbiol 67:541–557.

67. Dintilhac A, Claverys J-P. 1997. The adc locus, which affects competence for genetic transformation in *Streptococcus pneumoniae*, encodes an ABC transporter with a putative lipoprotein homologous to a family of streptococcal adhesins. Res Microbiol 148:119–131.

68. Loisel E, Jacquamet L, Serre L, Bauvois C, Ferrer JL, Vernet T, Di Guilmi AM, Durmort C. 2008. AdcAII, a new pneumococcal Zn-binding protein homologous with ABC transporters: biochemical and structural analysis. J Mol Biol 381:594–606.

69. Alloing G, de Philip P, Claverys J-P. 1994. Three highly homologous membrane-bound lipoproteins participate in oligopeptide transport by the Ami system of the Gram-positive *Streptococcus pneumoniae*. J Mol Biol 241:44–

907 58.
908 70. Alloing G, Trombe M, Claverys J-P. 1990. The *ami* locus of the Gram-positive
909 bacterium *Streptococcus pneumoniae* is similar to binding protein-dependent
910 transport operons of Gram-negative bacteria. Mol Microbiol 4:633–644.
911 71. Farshchi Andisi V, Hinojosa CA, de Jong A, Kuipers OP, Orihuela CJ, Bijlsma
912 JJE. 2011. Pneumococcal gene complex involved in resistance to extracellular
913 oxidative stress. Infect Immun 80:1037–1049.
914 72. Saleh M, Bartual SG, Abdullah MR, Jensch I, Asmat TM, Petruschka L, Pribyl
915 T, Gellert M, Lillig CH, Antelmann H, Hermoso JA, Hammerschmidt S. 2013.
916 Molecular architecture of *Streptococcus pneumoniae* surface thioredoxin-fold
917 lipoproteins crucial for extracellular oxidative stress resistance and
918 maintenance of virulence. EMBO Mol Med 5:1852–1870.
919 73. Härtel T, Klein M, Koedel U, Rohde M, Petruschka L, Hammerschmidt S.
920 2011. Impact of glutamine transporters on pneumococcal fitness under
921 infection-related conditions. Infect Immun 79:44–58.
922 74. Potter AJ, Trappetti C, Paton JC. 2012. *Streptococcus pneumoniae* uses
923 glutathione to defend against oxidative stress and metal ion toxicity. J Bacteriol
924 194:6248–6254.
925 75. Basavanna S, Khandavilli S, Yuste J, Cohen JM, Hosie AHF, Webb AJ,
926 Thomas GH, Brown JS. 2009. Screening of *Streptococcus pneumoniae* ABC
927 transporter mutants demonstrates that LivJHMGF, a branched-chain amino
928 acid ABC transporter, is necessary for disease pathogenesis. Infect Immun
929 77:3412–3423.
930 76. Weinrauch Y, Lacks SA. 1981. Nonsense mutations in the amylomaltase gene
931 and other loci in *Streptococcus pneumoniae*. Mol Gen Genet 183:7–12.

77. Basavanna S, Chimalapati S, Maqbool A, Rubbo B, Yuste J, Wilson RJ, Hosie A, Ogunniyi AD, Paton JC, Thomas G, Brown JS. 2013. The effects of methionine acquisition and synthesis on *Streptococcus pneumoniae* growth and virulence. PLoS One 8:e49638.
78. Adamou JE, Heinrichs JH, Erwin AL, Walsh W, Gayle T, Dormitzer M, Dagan R, Brewah YA, Barren P, Lathigra R, Langermann S, Koenig S, Johnson S. 2001. Identification and characterization of a novel family of pneumococcal proteins that are protective against sepsis. Infect Immun 69:949–958.
79. Brown JS, Gilliland SM, Holden DW. 2001. A *Streptococcus pneumoniae* pathogenicity island encoding an ABC transporter involved in iron uptake and virulence. Mol Microbiol 40:572–585.
80. Brown JS, Gilliland SM, Ruiz-Albert J, Holden DW. 2002. Characterization of Pit, a *Streptococcus pneumoniae* iron uptake ABC transporter. Infect Immun 70:4389–4398.
81. Bidossi A, Mulas L, Decorosi F, Colomba L, Ricci S, Pozzi G, Deutscher J, Viti C, Oggioni MR. 2012. A functional genomics approach to establish the complement of carbohydrate transporters in *Streptococcus pneumoniae*. PLoS One 7:e33320.
82. Saxena S, Khan N, Dehinwal R, Kumar A, Sehgal D. 2015. Conserved surface accessible nucleoside ABC transporter component SP0845 is essential for pneumococcal virulence and confers protection *in vivo*. PLoS One 10:e0118154.
83. Cron LE, Bootsma HJ, Noske N, Burghout P, Hammerschmidt S, Hermans PWM. 2009. Surface-associated lipoprotein PpmA of *Streptococcus pneumoniae* is involved in colonization in a strain-specific manner.

Microbiology 155:2401–2410.

84. Orihuela CJ, Mills J, Robb CW, Wilson CJ, Watson DA, Niesel DW. 2001. *Streptococcus pneumoniae* PstS production is phosphate responsive and enhanced during growth in the murine peritoneal cavity. Infect Immun 69:7565–7571.

85. Hermans PWM, Adrian P V, Albert C, Estevão S, Hoogenboezem T, Luijendijk IHT, Kamphausen T, Hammerschmidt S. 2006. The Streptococcal Lipoprotein Rotamase A (SlrA) is a functional peptidyl-prolyl isomerase involved in pneumococcal colonization. J Biol Chem 281:968–976.

86. Moscoso M, García E, López R. 2006. Biofilm formation by Streptococcus pneumoniae: Role of choline, extracellular DNA, and capsular polysaccharide in microbial accretion. J Bacteriol 188:7785–7795.

87. Granok AB, Parsonage D, Ross RP, Caparon MG. 2000. The RofA binding site in Streptococcus pyogenes is utilized in multiple transcriptional pathways. J Bacteriol 182:1529–1540.

FIGURE LEGENDS

Figure 1. Pneumococcal *lgt* mutants were less inflammatory compared to WT strains. (A) SEAP reporter readout from HEK-Blue™ hTLR2 reporter cells treated with pneumococcal strains at MOI 10 for 16 hours. (B) Expression of a transcriptional module reflective of TLR2-mediated activity in Detroit 562 cells infected with TIGR4 and BHN418 for 3 hours. (C-F) Transcript levels of (C) *CXCL10*, (D) *IFNB1*, (E) *IFNL1* and (F) *IFNL3,* quantified via qPCR using total RNA extracted from Detroit 562 cells after 6 hours of infection with pneumococcal strains. Statistical significance was determined using multiple comparison test with Bonferroni's correction (A), Mann-Whitney test (B), or Student's *t*-test assuming equal variance (C-F). * indicates $p < 0.05$, ** indicates $p < 0.01$, *** indicates $p < 0.001$, *** indicates $p < 0.0001$.

Figure 2. Mutation of *lgt* impaired epithelial microinvasion by *Streptococcus pneumoniae*, with greater defects for BHN418. (A-F) NPE microinvasion by WT and *lgt* mutants. Graphs show CFU numbers for BHN418-derived (A-C) and TIGR4-derived strains (D-F) associated with (A,D), internalised into (B,E), or growing in proximity with Detroit 562 NPE cells 3 hours post infection. * indicates $p < 0.05$, ** indicates $p < 0.01$, *** indicates $p < 0.001$.

Figure 3. Growth of BHN418 *lgt::cm* compared to WT. (A-B) Growth of BHN418-derived (A) and TIGR4-derived (B) strains in infection medium (MEM + 1% FBS) in the presence of Detroit 562 NPE cells. (C-D) Growth of BHN418-derived strains in infection medium (C) and in the rich growth medium THY (D) in the absence of cells. * indicates $p < 0.05$ by Student's *t*-test.

Figure 4. PalA is a lipoprotein present in BHN418 but not in TIGR4. (A) Genetic context of the *palA* gene (black arrow), which is within a multi-gene operon that is part of a putative genetic island. ORFs with homology to previously described genes are labelled with the gene name. (B) Predicted structure of PalA, modelled using AlphaFold2, which shows two subdomains connected by a hinge region with a possible central ligand binding pocket. The extended stalk-like structure contains the signal peptide and lipoprotein processing sequence and is likely cleaved/absent in the mature lipoprotein.

Figure 5. PalA was not essential for NPE microinvasion, murine colonisation and progression to disease. (A-C) NPE microinvasion by WT BHN418 and *palA* mutants, measured as NPE-associated bacteria (A), internalised bacteria (B) and planktonic bacteria growing in proximity with Detroit 562 NPE cells 3 hours post infection. (D-E) Growth of WT BHN418, the *palA* knock out and complementation mutants in THY (D) and infection medium (E). (F-I) Recovery of pneumococci from mice intranasally inoculated with WT BHN418 and *palA::kan* mutant, recovered from nasal washes when inoculated singly (F) or competitively in a 1:1 ratio (G), as well as from the lungs (H) and bloodstream (I) when tested on a pneumonia model. * indicates $p < 0.05$.

Figure 6. Heterologous expression of *palA* in P1121 (serotype 23F) did not increase epithelial microinvasion or TLR2 signalling. (A-C) NPE microinvasion by WT P1121 and *palA* expression mutants, measured as NPE-associated bacteria (A), internalised bacteria (B) and planktonic bacteria growing in proximity with Detroit

562 NPE cells 3 hours post infection. (D) SEAP reporter readout from HEK-Blue™ hTLR2 reporter cells treated with pneumococcal strains at MOI 10 for 16 hours.

Table 1. Lipoproteins encoded by TIGR4 and BHN418, identified bioinformatically using MEME suite.

BHN418 locus tag	TIGR4 locus tag	Gene name	Description of gene product	Reference
RSS80_07140	SP_1500	*aatB*	Amino acid transporter	(66)
RSS80_10715	SP_2169	*adcA*	Adhesin competence protein A; zinc transporter	(67)
RSS80_04890	SP_1002	*adcAII*	Adhesin competence protein AII; zinc transporter	(68)
RSS80_01875	SP_0366	*aliA*	AmiA-like protein A; oligopeptide transporter	(69)
RSS80_07270	SP_1527	*aliB*	AmiA-like protein B; oligopeptide transporter	(69)
RSS80_09070	SP_1891	*amiA*	Aminopterin resistance locus protein A; oligopeptide transporter	(70)
RSS80_03115	SP_0629	*dacB*	L,D-carboxypeptidase	(10)
RSS80_03240	SP_0659	*etrx1*	Extracellular thioredoxin-like protein 1; thiol-disulfide oxidoreductase	(71)
RSS80_04875	SP_1000	*etrx2*	Extracellular thioredoxin-like protein 2; thiol-disulfide oxidoreductase	(72)
RSS80_06715	SP_1394	*glnH*	GlnH glutamine/polar amino acid ABC transporter substrate-binding protein	(73)
RSS80_00785	SP_0148	*gshT*	Glutathione transporter	(74)
RSS80_03685	SP_0749	*livJ*	Branched chain amino-acid transporter	(75)
RSS80_10385	SP_2108	*malX*	Maltosaccharide transporter	(76)
RSS80_00790	SP_0149	*metQ*	Methionine-binding lipoprotein Q	(77)
RSS80_05810	SP_1175	*phtA*	Pneumococcal histidine triad protein A	(78)
RSS80_05040	SP_1032	*piaA*	Pneumococcal iron acquisition protein A	(79)
RSS80_01305	SP_0243	*pitA*	Pneumococcal iron transporter protein A	(80)
RSS80_08955	SP_1872	*piuA*	Pneumococcal iron uptake protein A	(79)
RSS80_04120	SP_0845	*pnrA*	Nucleoside transporter	(81, 82)
RSS80_04795	SP_0981	*ppmA*	Putative proteinase maturation protein A; peptidyl-prolyl cis–trans isomerase	(83)
RSS80_07850	SP_1650	*psaA*	Pneumococcal surface adhesin A; manganese and zinc transporter	(11, 12)
RSS80_10265	SP_2084	*pstS*	Phosphate transport substrate binding protein	(84)
RSS80_09095	SP_1897	*rafE*	Raffinose transporter	(27)
RSS80_03790	SP_0771	*slrA*	Streptococcal lipoprotein rotamase A;cyclophilin-type peptidyl-prolyl cis–trans isomerase	(85)
RSS80_04895[§]	SP_1003	*phtB*	Pneumococcal histidine triad protein B	(78)
RSS80_04895[§]	SP_1174	*phtD*	Pneumococcal histidine triad protein D	(78)
RSS80_06745	SP_1400	*pstS2*	phosphate binding protein	-
RSS80_10885	SP_2197	-	ABC transporter binding protein	-
RSS80_00530	SP_0112	-	Amino acid binding protein	-
RSS80_09960	SP_2041	-	Membrane protein insertase	-

RSS80_04185	SP_0857*	-	ABC transporter substrate binding protein	-
RSS80_03070	SP_0620	-	Amino acid ABC transporter binding protein	-
RSS80_09570	SP_1975	-	Membrane protein insertase	-
RSS80_03435*	SP_0708*	-	ABC transporter substrate binding protein (truncated)	-
RSS80_03595	**Not present**	**-**	**Extracellular solute binding protein**	**-**
RSS80_04430	SP_0899	-	Hypothetical protein	-
RSS80_05800*	Not assigned	-	ABC transporter substrate binding protein (truncated)	-
RSS80_08015	SP_1683	-	ABC transporter sugar binding protein	-
RSS80_08055	SP_1690	-	ABC transporter sugar binding protein	-
RSS80_08595	SP_1796	-	Extracellular solute binding protein	-
RSS80_08765	SP_1826	-	ABC transporter substrate binding protein	-
RSS80_00445	SP_0092	-	ABC transporter substrate binding protein	-
RSS80_01055	SP_0191	-	Hypothetical protein	-
RSS80_01080	SP_0198	-	ABC transporter substrate binding protein	-

[bold] ORF present in BHN418 but not TIGR4.
* Annotated as pseudogene, contained premature stop codon, or interrupted by insertion sequence
§ RSS80_04895 was the best match BLAST result for more than one TIGR4 CDS
Not assigned: Homologous sequence present in genome but not annotated as ORF/CDS
Not present: Homologous sequence absent in genome.
TIGR locus tag and gene name are based on TIGR4 genome annotation (Genbank accession number AE005672.3).

Table 2. Presence of *palA* in whole genome sequences of pneumococcal isolates on the BIGSdb database, stratified by site of isolation ("source").

Category	Source (BIGSdb label)	Proportion (%)
Carriage	"nasopharynx", "pharynx", "sputum"	14.57 (3114/21369)
Otitis	"ear swab", "middle ear fluid"	13.72 (129/940)
Pneumonia	"lung aspirate", "sinus aspirate", "bronchoalveolar lavage", "bronchi"	8.96 (25/279)
Invasive	"blood", "cerebrospinal fluid", "joint fluid", "pleural fluid	6.54 (1837/28075)
Eye/pus/others	"eye swab", "pus", "other"	2.65 (19/716)
Overall		9.97 (5124/51379)

Table 3. Bacterial strains and plasmids used in this study.

Designation	Genotype/ Description	Source
Strains		
TIGR4	WT Serotype 4 isolate	(29)
BHN418	WT Serotype 6B isolate	(16)
P1121	WT Serotype 23F isolate	(2)
ECSPN100	TIGR4 *lgt::cm*	This work
ECSPN106	TIGR4 *lgt::cm* P_{IPTG}-*lgt-erm* (TIGR4 *lgt* complementation)	This work
ECSPN200	BHN418 *lgt::cm*	This work
ECSPN210	BHN418] *lgt::cm* P_{IPTG}-*lgt-erm* (BHN418 *lgt* complementation)	This work
ECSPN211	BHN418 *palA::kan*	This work
ECSPN213	BHN418 *palA::kan* P_{IPTG}-*palA-erm* (BHN418 *palA* complementation)	This work
ECSPN400	P1121 P_{IPTG}-*palA-erm*	This work
ECSPN401	P1121 P_{palA}-*palA-kan*	This work
Plasmids		
pASR103	Complementation construct with an IPTG inducible promoter and *erm* selectable marker	(47)
pPEPY	Complementation construct with a *kan* selectable marker	(47)
pEMcat	Minitransposon plasmid; source of cm^R cassette	(86)
pABG5	Cloning plasmid; source of kan^R cassette	(87)
pEC210	TIGR4 *lgt* coding region cloned into pASR103	This work
pEC211	BHN418 *lgt* coding region cloned into pASR103	This work
pEC213	BHN418 *palA* coding region cloned into pASR103	This work
pEC213	BHN418 *palA* promoter and coding region cloned into pPEPY	This work

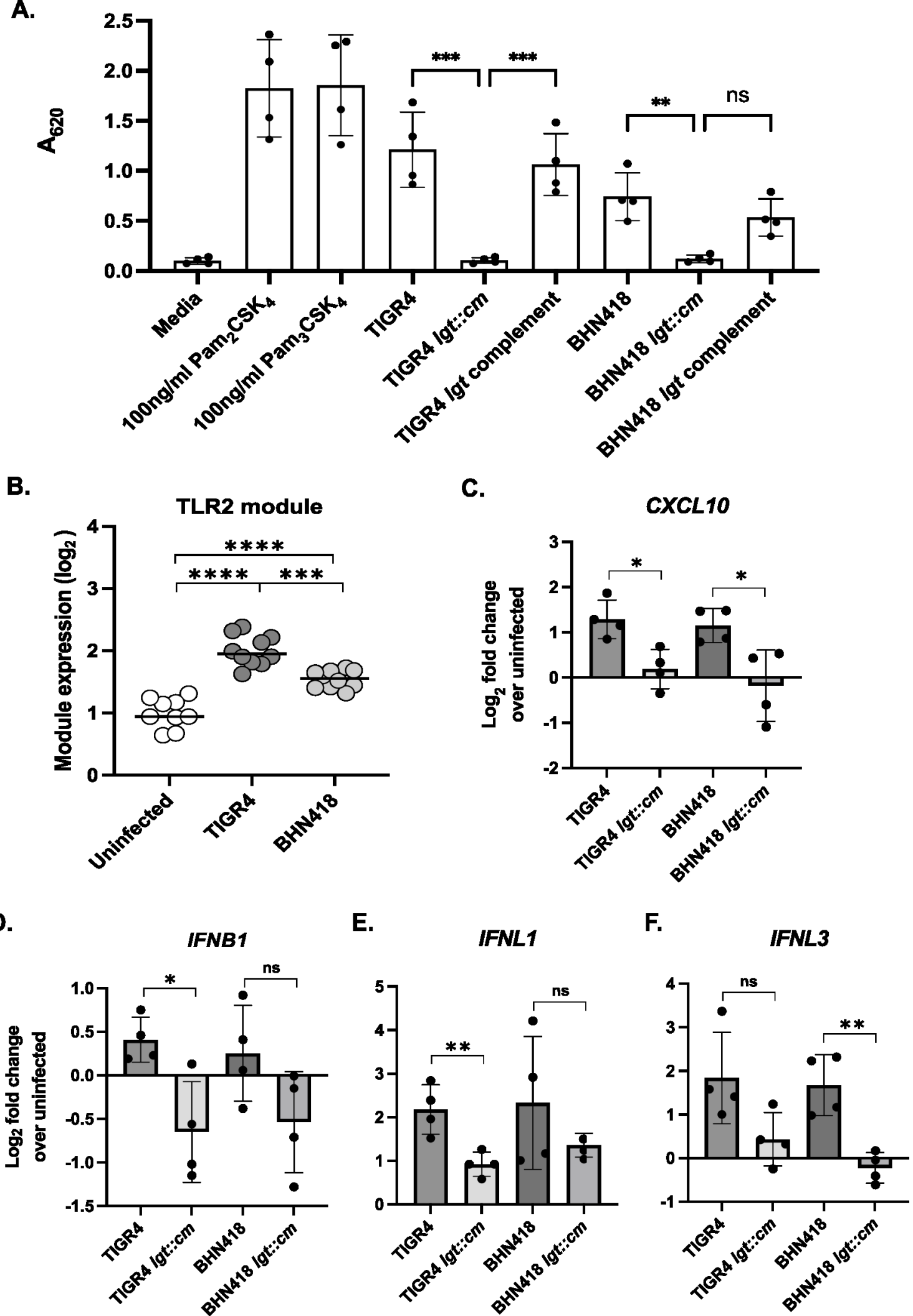
A.
A_{620}
2.5
2.0
1.5
1.0
0.5
0.0
***
***
**
ns
Media
100ng/ml Pam_2CSK_4
100ng/ml Pam_3CSK_4
TIGR4
TIGR4 *lgt::cm*
TIGR4 *lgt* complement
BHN418
BHN418 *lgt::cm*
BHN418 *lgt* complement
B.
TLR2 module
Module expression (log_2)
4
3
2
1
0
****
****
***
Uninfected
TIGR4
BHN418
C.
CXCL10
Log_2 fold change over uninfected
3
2
1
0
-1
-2
*
*
TIGR4
TIGR4 *lgt::cm*
BHN418
BHN418 *lgt::cm*
D.
IFNB1
Log_2 fold change over uninfected
1.0
0.5
0.0
-0.5
-1.0
-1.5
*
ns
TIGR4
TIGR4 *lgt::cm*
BHN418
BHN418 *lgt::cm*
E.
IFNL1
5
4
3
2
1
0
**
ns
TIGR4
TIGR4 *lgt::cm*
BHN418
BHN418 *lgt::cm*
F.
IFNL3
4
3
2
1
0
-1
ns
**
TIGR4
TIGR4 *lgt::cm*
BHN418
BHN418 *lgt::cm*

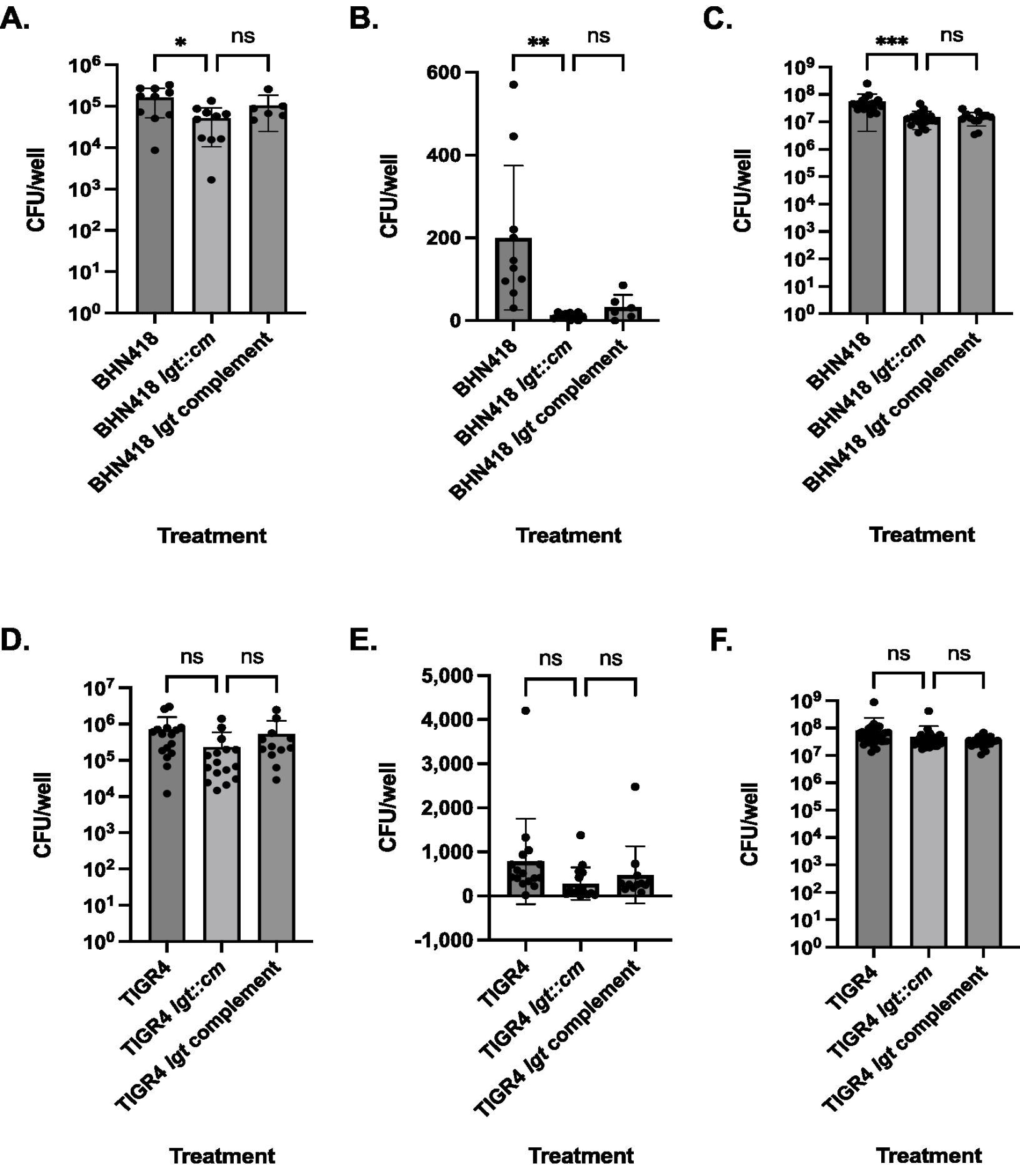
A.
B.
C.
D.
E.
F.
CFU/well
Treatment
BHN418
BHN418 lgt::cm
BHN418 lgt complement
TIGR4
TIGR4 lgt::cm
TIGR4 lgt complement
ns
*
**
***

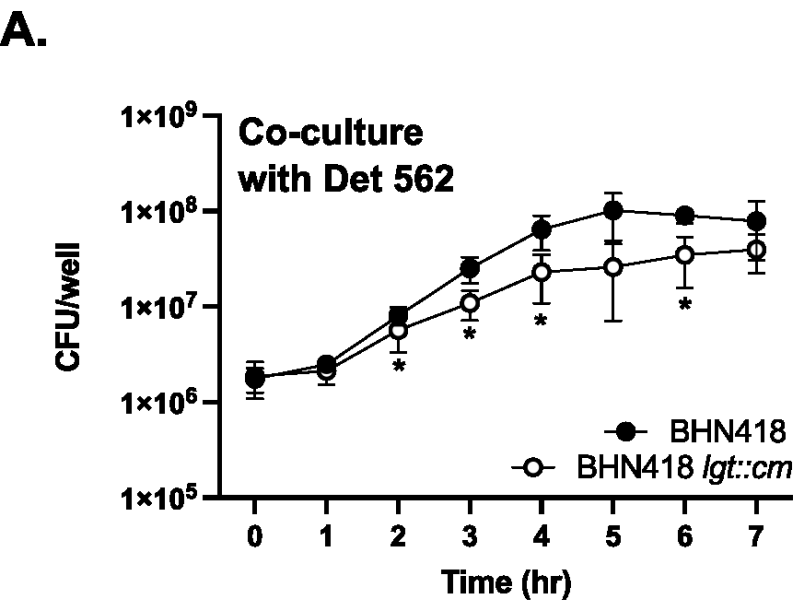
A.
Co-culture
with Det 562
CFU/well
1×10^9
1×10^8
1×10^7
1×10^6
1×10^5
0 1 2 3 4 5 6 7
Time (hr)
BHN418
BHN418 lgt::cm

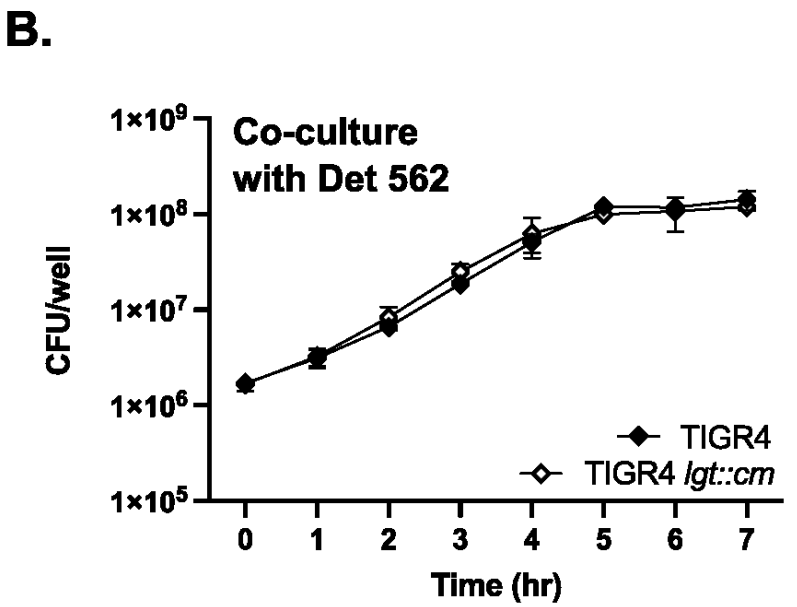
B.
Co-culture
with Det 562
CFU/well
1×10^9
1×10^8
1×10^7
1×10^6
1×10^5
0 1 2 3 4 5 6 7
Time (hr)
TIGR4
TIGR4 lgt::cm

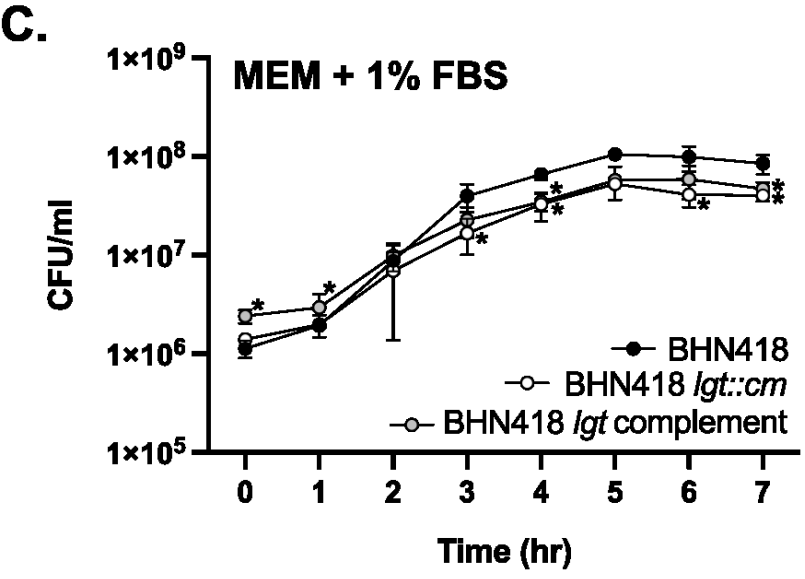
C.
MEM + 1% FBS
CFU/ml
1×10^9
1×10^8
1×10^7
1×10^6
1×10^5
0 1 2 3 4 5 6 7
Time (hr)
BHN418
BHN418 lgt::cm
BHN418 lgt complement

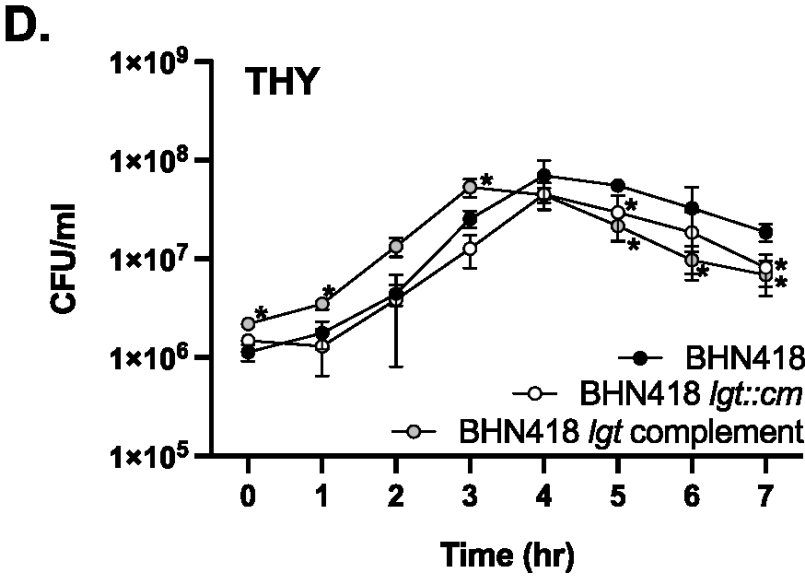
D.
THY
CFU/ml
1×10^9
1×10^8
1×10^7
1×10^6
1×10^5
0 1 2 3 4 5 6 7
Time (hr)
BHN418
BHN418 lgt::cm
BHN418 lgt complement

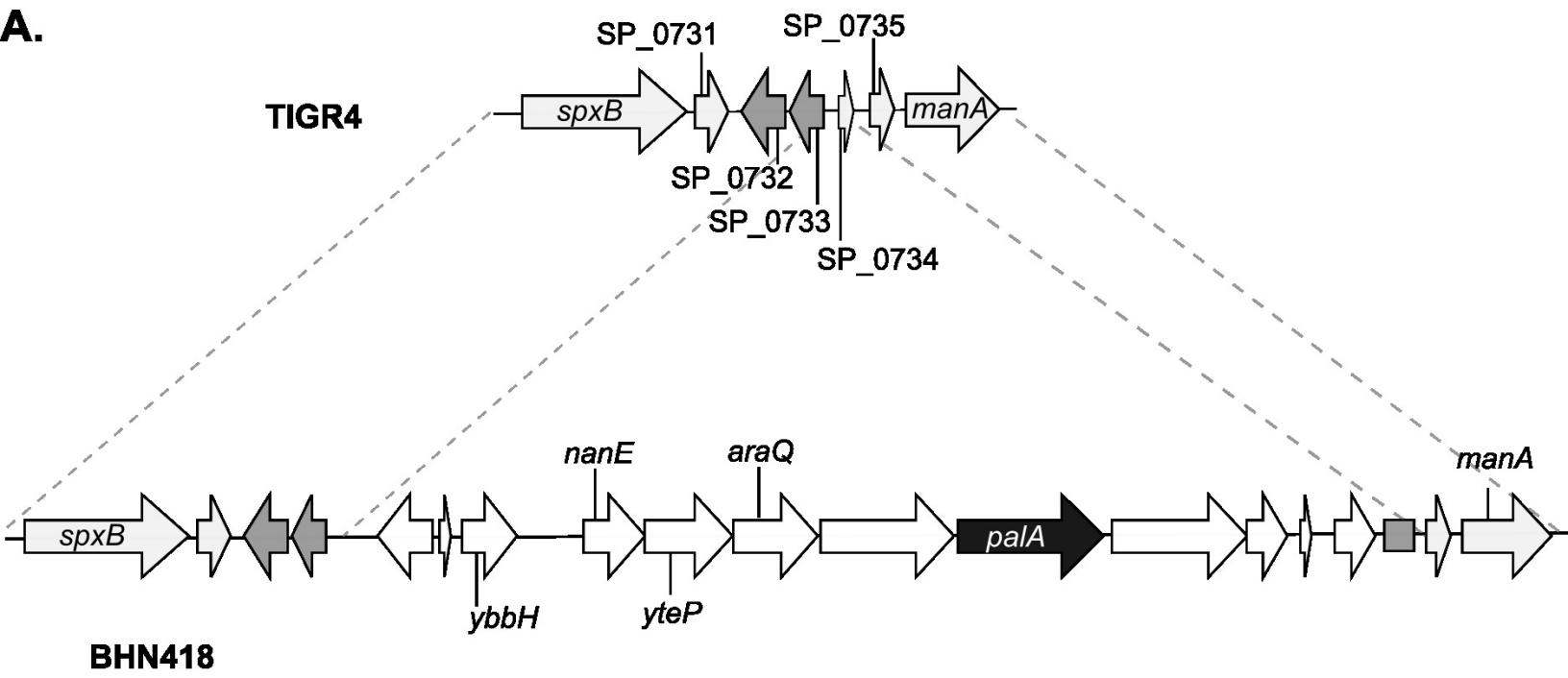
A.
TIGR4
SP_0731
SP_0735
spxB
manA
SP_0732
SP_0733
SP_0734
nanE
araQ
manA
spxB
palA
ybbH
yteP
BHN418

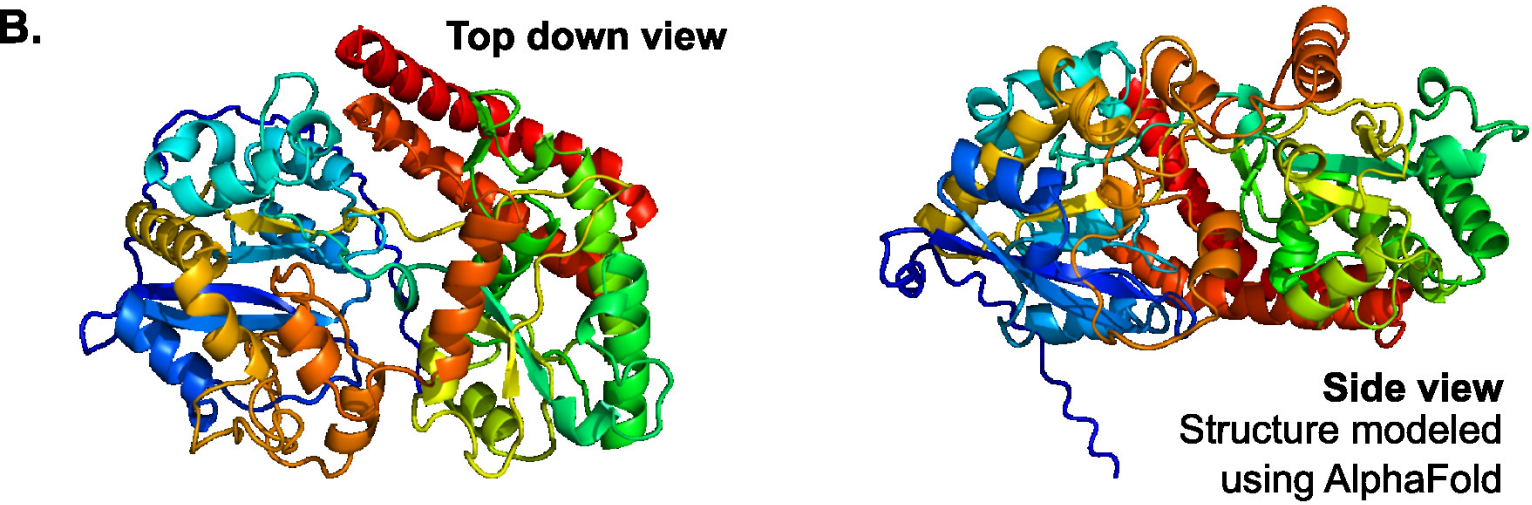
B.
Top down view
Side view
Structure modeled
using AlphaFold

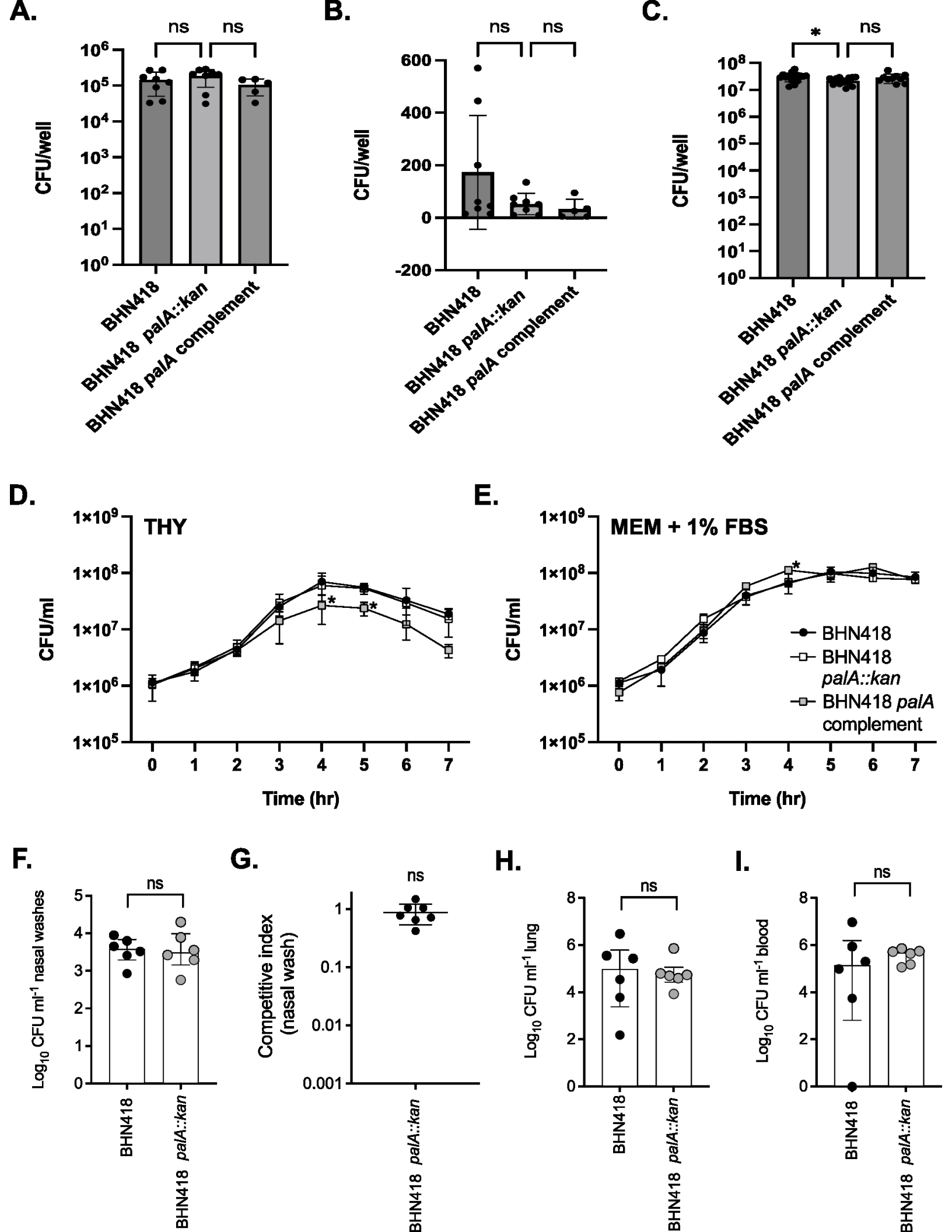
A.
B.
C.
ns
*
CFU/well
BHN418
BHN418 palA::kan
BHN418 palA complement
D.
E.
THY
MEM + 1% FBS
CFU/ml
Time (hr)
BHN418
BHN418 palA::kan
BHN418 palA complement
F.
G.
H.
I.
Log10 CFU ml-1 nasal washes
Competitive index (nasal wash)
Log10 CFU ml-1 lung
Log10 CFU ml-1 blood

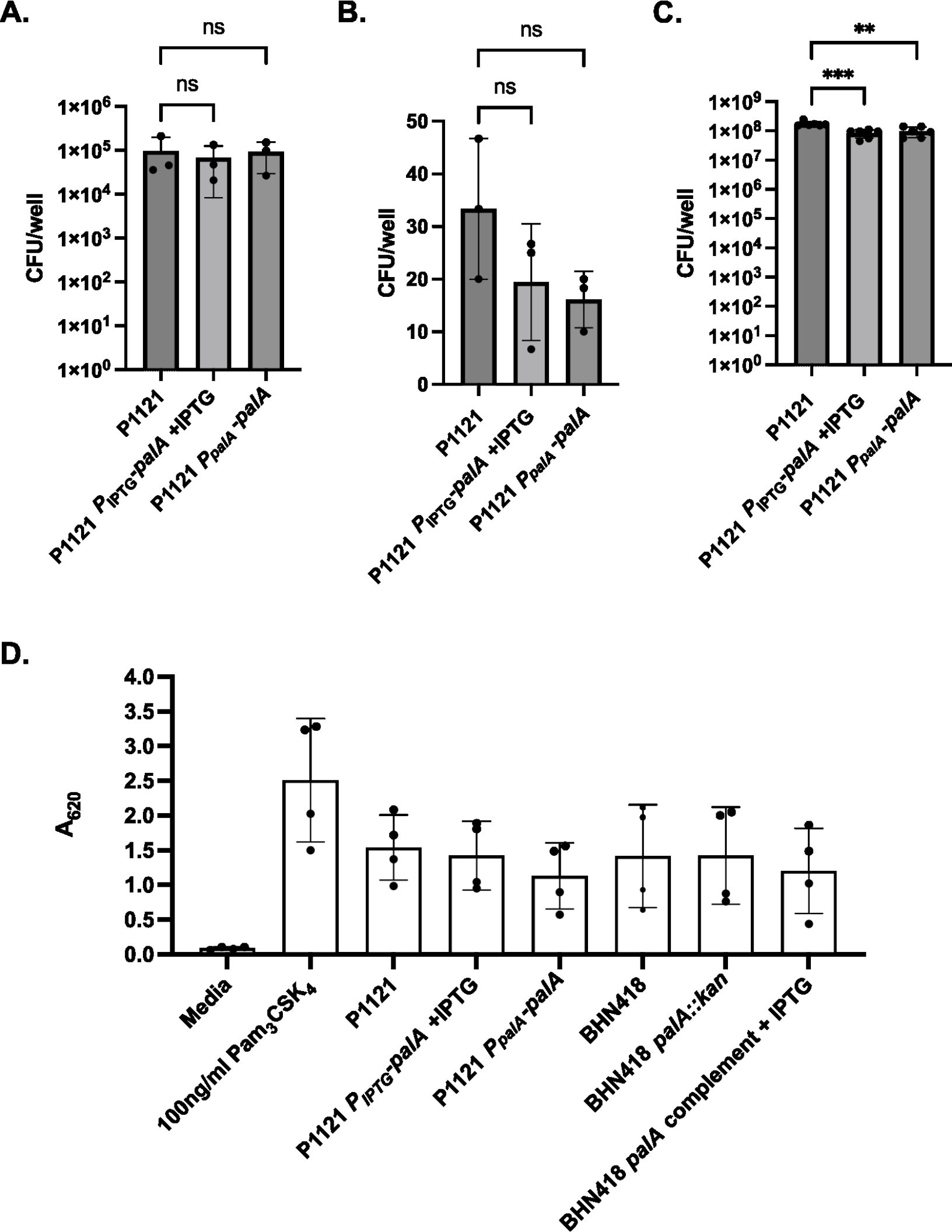
A.
ns
ns
CFU/well
1×10^6
1×10^5
1×10^4
1×10^3
1×10^2
1×10^1
1×10^0
P1121
P1121 P_IPTG-palA +IPTG
P1121 P_palA-palA
B.
ns
ns
CFU/well
50
40
30
20
10
0
P1121
P1121 P_IPTG-palA +IPTG
P1121 P_palA-palA
C.
**
***
CFU/well
1×10^9
1×10^8
1×10^7
1×10^6
1×10^5
1×10^4
1×10^3
1×10^2
1×10^1
1×10^0
P1121
P1121 P_IPTG-palA +IPTG
P1121 P_palA-palA
D.
A620
4.0
3.5
3.0
2.5
2.0
1.5
1.0
0.5
0.0
Media
100ng/ml Pam3CSK4
P1121
P1121 P_IPTG-palA +IPTG
P1121 P_palA-palA
BHN418
BHN418 palA::kan
BHN418 palA complement + IPTG